



## ORIGINAL RESEARCH COMMUNICATION

# Nattokinase's Neuroprotective Mechanisms in Ischemic Stroke: Targeting Inflammation, Oxidative Stress, and Coagulation

Xin-ying Yang, Sheng-lin Wang, Wen-chi Xue, Yu-peng Zhang, Liang-liang Li, Zhao-hu Luo, and Feng-jiao Zhang

### Abstract

**Aims:** Nattokinase (NK), a potent serine endopeptidase, has exhibited a variety of pharmacological effects, including thrombolysis, anti-inflammation, and antioxidative stress. Building on previous research highlighting NK's promise in nerve regeneration, our study investigated whether NK exerted protective effects in transient middle cerebral artery occlusion (tMCAO)-induced cerebral ischemia-reperfusion injury and the underlying mechanisms.

**Results:** The rats were administered NK (5000, 10000, 20000 FU/kg, i.g., 7 days before surgery, once daily). We showed that NK treatment dose dependently reduced the infarction volume and improved neurological symptoms, decreased the proinflammatory and coagulation cytokines levels, and attenuated reactive oxygen species (ROS) in the infarcted area of tMCAO rats. We also found that NK could exert neuroprotective effects in a variety of vitro models, including the microglia inflammation model and neuronal oxygen-glucose deprivation/reperfusion (OGD/R) model. Notably, NK effectively countered OGD/R-induced neuron death, modulating diverse pathways, including autophagy, apoptosis, PARP-dependent death, and endoplasmic reticulum stress. Furthermore, the neuroprotection of NK was blocked by phenylmethylsulfonyl fluoride (PMSF), a serine endopeptidase inhibitor. We revealed that heat-inactive NK was unable to protect against tMCAO injury and other vitro models, suggesting NK attenuated ischemic injury by its enzymatic activity. We conducted a proteomic analysis and found inflammation and coagulation were involved in the occurrence of tMCAO model and in the therapeutic effect of NK.

**Innovation and Conclusion:** In conclusion, these data demonstrated that NK had multifaceted neuroprotection in ischemic brain injury, and the therapeutic effect of NK was related with serine endopeptidase activity.

**Keywords:** ischemic stroke, Nattokinase, inflammation, ROS, TLR4

### Introduction

Ischemic stroke (IS) is the second leading cause of mortality and a significant contributor to disability, presents formidable challenges due to the scarcity of effective treatment options (Ajoolabady et al., 2021). At present, tissue plasminogen activator (tPA) is the only FDA-approved medication, with its therapeutic window restricted to 4.5 h for eligible individuals (Sarvari et al., 2020). Unfortunately, only a fraction of patients with IS benefit from thrombolytic therapy.

Furthermore, treatment with tPA or surgical interventions can aggravate blood-brain barrier disruption and increase the risk of hemorrhagic transformation (Sumii and Lo, 2002; Wang et al., 2015). Therefore, there is an urgent need to foster innovation and develop safe and effective pharmacological interventions aimed at preventing stroke.

Brain injury following stroke is a complex process influenced by various pathological mechanisms, including coagulation, inflammation, oxidative stress, and apoptosis (Iadecola and Anrather, 2011). Accumulating evidence

### Innovation

Nattokinase (NK) is a serine endopeptidase with multiple protective effects, including anti-inflammation and antithrombus. However, less is known about the protective impact of this pharmacological strategy in the context of IS. This study demonstrated that NK may play a protective role by inhibiting microglial inflammation, oxidative stress, and neuronal cell death in IS. The detection of the mechanism showed that NK could degrade TLR4 protein through its enzymatic activity (Fig. 1).

indicates that the existence of intricate crosstalk between the systems of inflammation and coagulation, in which inflammatory responses trigger the activation of coagulation and vice versa, lead to a reciprocal impact on their respective activities. In the context of ischemia–reperfusion injury, immune cells can engage in intricate interactions with platelets, facilitating the formation of infarctions (Stoll and Nieswandt, 2019). For example, lipopolysaccharide (LPS) administration has been shown to significantly increase endothelial cell-type plasminogen activator inhibitor-1 (PAI-1) level in the brain, plasma, and liver of rats, thus inducing activation of glomerular fibrinogen (FIB) (Tsantarliotou et al., 2019). Among the potent endogenous inhibitors of FIB activator, PAI-1 plays a crucial role in the development of infectious shock and thromboembolic disease (Wang et al., 2020). Furthermore, inflammatory factors, including tumor necrosis factor- $\alpha$  (TNF- $\alpha$ ), contribute to the dynamic interaction between inflammation and thrombosis. TNF- $\alpha$  promotes macrophage activation, leading to the release of inflammatory factors such as interleukin (IL)-6 and IL-1 $\beta$ , these factors, in turn, promote endothelial damage and thrombosis in the body. In addition, TNF- $\alpha$  also decreases the release of plasminogen activator (tPA) from monocytes and endothelial cells, while increasing the synthesis and release of tissue factor, promoting thrombosis (Chanchal et al., 2020). These cytokines stimulate the production of tissue factor in mononuclear cells, which results in systemic activation of coagulation in severe sepsis (McDonald et al., 2017). Acute arterial thrombotic events follow from thrombus formation at the site of a ruptured atherosclerotic plaque, characterized by an abundance of inflammatory cells (Opal and Esmon, 2003). Modulation of inflammation is primarily dependent on the role of coagulation proteases, which bind to protease-activated receptors (PARs). Activation of PARs through binding of thrombin to its cellular receptor elicits the release of various cytokines and growth factors, including TNF- $\alpha$  and IL-1 $\beta$  (Levi and van der Poll, 2010). In particular, blood clots have the potential to fuel inflammation. Activated platelets are known to participate in the inflammatory processes associated with atherosclerosis. Systemic coagulation activation and microvascular failure can occur as a consequence of a systemic inflammatory response triggered by severe infection or sepsis (Levi et al., 2004). In fact, oxygen-free radicals are responsible for the oxidation of neuronal lipids, proteins, and nucleic acids, which in turn contributes to oxidative damage to the brain (Lin et al., 2019). As a consequence of reactive oxygen species (ROS), platelets become more susceptible to

platelet-aggregating agents, such as thrombin, collagen, and arachidonic acid, and leukocytes become more activated (Masselli et al., 2020). Given these considerations, it is reasonable to propose therapeutic regimens targeting coagulation, oxidative stress, and inflammation, rather than employing specific therapies, which may offer enhanced efficacy.

Nattokinase (NK), a 26 kDa serine protease extracted from the traditional Japanese food known as Natto, is beneficial for cardiovascular disease due to its extraordinary thrombolytic and anticoagulant properties (Kim et al., 2008; Wu et al., 2019). In a previous investigation, we confirmed that NK did not have genotoxicity in mice, with the maximum daily tolerant dose of 480000 FU/kg, which is 1000 times higher than the recommended daily dose for humans (Wu et al., 2019). Our previous study demonstrated that NK improved LPS-activated macrophage signaling, providing protection against LPS-induced acute kidney injury (AKI) and glomerular thrombus formation in mice. Notably, NK disrupted the detrimental cycle involving inflammation, oxidative stress, and thrombosis (Wu et al., 2020). In addition, a recent study also illustrates NK's protective role against acute IS and its impressive promotion of neurogenesis in rat models by increasing peripheral blood irisin, leading to enhanced cognitive functions (Wu et al., 2023). Nevertheless, the specific mechanism underlying NK's protection against IS, especially its properties against inflammatory and antioxidant stress as an effective antithrombotic agent, remains uncertain. To address this critical knowledge gap, our current investigation comprehensively examined the impact of NK on multiple IS models both *in vivo* and *in vitro*. Our findings indicated the protective effect of NK against transient middle cerebral artery occlusion (tMCAO)-induced damage, microglial inflammation, and neuronal death (Fig. 1). Importantly, NK effectiveness was closely correlated with its serine endopeptidase activity and TLR4 proteolysis.

## Results

### *NK protected against tMCAO-induced brain injury and improved neurological function*

In recent research, we discovered that pretreatment with NK had a remarkable positive impact on mitigating cerebral infarction induced by permanent middle cerebral artery occlusion (pMCAO) rats (Wu et al., 2023). However, it remained unclear whether NK also held potential to effectively protect against brain injury caused by tMCAO. As shown in Figure 2A, the group subjected to sham operation exhibited no signs of infarction. Conversely, the tMCAO group displayed significantly larger infarct volumes compared with the sham group. Intriguingly, pretreatment with NK led to a reduction in cerebral infarct size within the tMCAO group in a dose-dependent pattern. Furthermore, NK alleviated brain water content of rats following tMCAO (Fig. 2B). To evaluate the impact of NK on neurological function subsequent to tMCAO, several tests were conducted, including the modified neurological severity score (mNSS), the rotarod test, and the cylinder test. Notably, NK administration substantially improved neurological function when contrasted with the

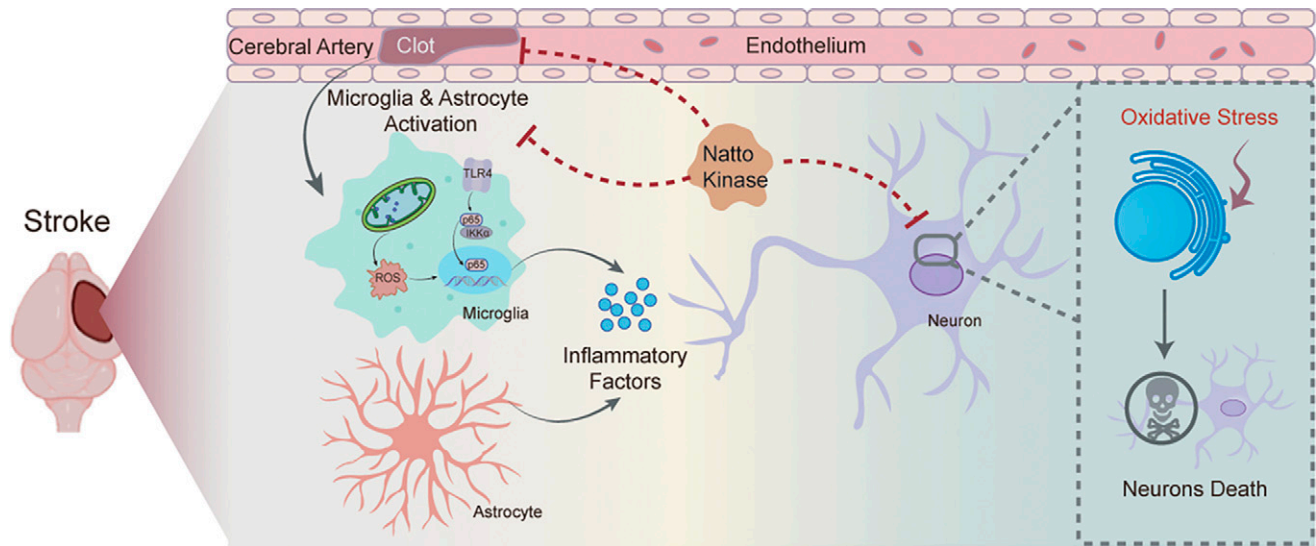


**FIG. 1. Graphic summary illustration.** The schematic of the novel neuroprotective insight of NK targeting inflammation, oxidative stress, and coagulation. NK inhibited the activation of microglia and astrocyte and the released of inflammatory cytokines through NF- $\kappa$ B signaling pathways, further reducing inflammatory cytokine-induced neuronal damage. In addition, NK can effectively inhibit neuron death and play a diverse role in neuroprotection. NK, nattokinase; NF, nuclear factor.

tMCAO condition (Fig. 2C). Furthermore, results from motor function tests confirmed that tMCAO rats exhibited a shorter duration of maximal speed rotation in comparisons to the sham group. NK treatment improved the rotation

duration among tMCAO rats (Fig. 2D). In addition, the cylinder test revealed a reduction in ipsilateral forepaw preference in rats treated with NK, in contrast to the tMCAO group, at 24 h post tMCAO (Fig. 2E). In summary, these results

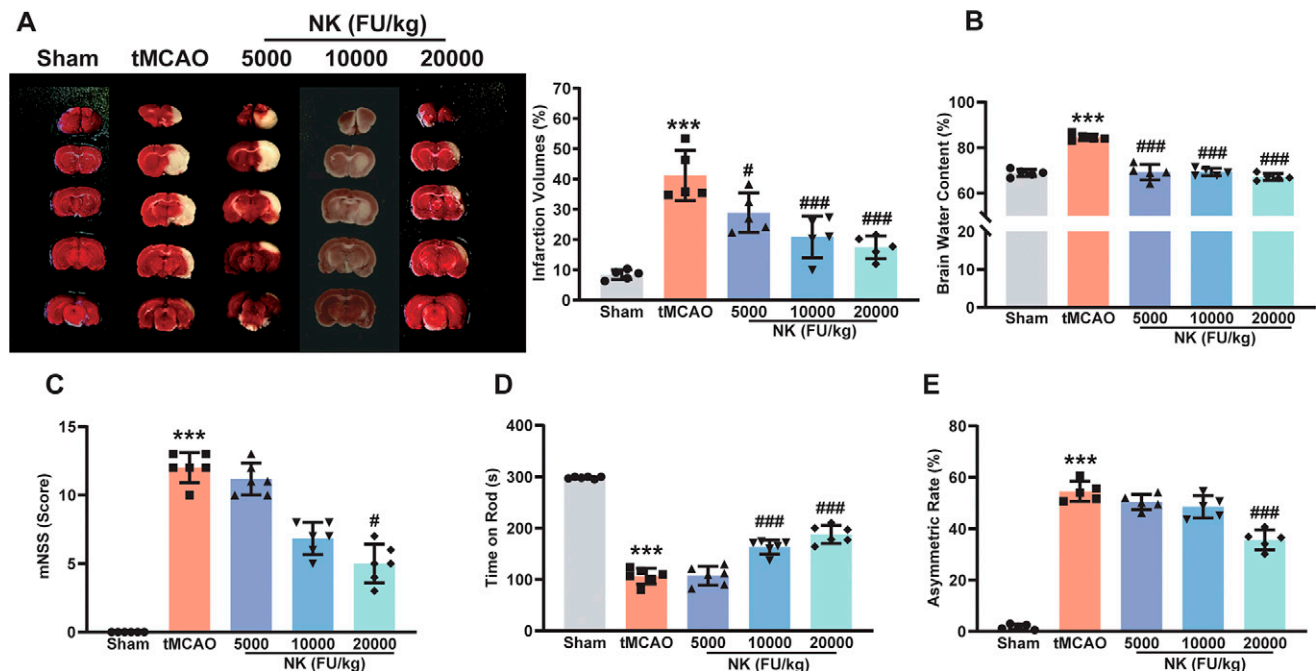


**FIG. 2. NK reduced tMCAO-induced brain injury and improved neurological function in rats.** Rats were administered with NK orally at doses of 5000, 10000, and 20000 FU/kg for 7 days before induction of tMCAO induction. (A) TTC staining of the brain and quantification of infarct volumes 24 h after tMCAO. (B) Brain water content was measured 24 h after tMCAO. Sensorimotor functions were evaluated by (C) mNSS, (D) rotarod test, and (E) cylinder test after tMCAO. The values were expressed as means  $\pm$  SD. Statistical analysis was performed with one-way ANOVA followed by Tukey. The graph C was analyzed by nonparametric test. \*\*\* $p$  < 0.001 versus Sham group; # $p$  < 0.05, ### $p$  < 0.001 compared with tMCAO group ( $n$  = 5–6). ANOVA, analysis of variance; mNSS, modified neurological severity score; tMCAO, transient middle cerebral artery occlusion, TTC, 2,3,5-triphenyltetrazolium chloride solution.

demonstrated the efficacy of NK pre-administration in ameliorating neurological deficits and reducing the extent of IS injury in rats following tMCAO.

#### *NK suppressed proinflammatory cytokine release in tMCAO rats and BV2 cells*

Following stroke, the initial ischemic injury coupled with reperfusion injury results in the release of various inflammatory cytokines within the brain, thereby triggering neuroinflammation. NK has been attributed with anti-inflammatory properties of NK due to its impact on thrombus formation (Wu et al., 2020). In this context, we measured the concentrations of both TNF- $\alpha$  and IL-10 in both the ipsilateral hemisphere and serum. As illustrated in Figure 3, NK not only lowered the systemic levels of TNF- $\alpha$  and IL-10 subsequent to tMCAO (Fig. 3A and Fig. 3B), but also impressively diminished tMCAO-induced TNF- $\alpha$  and IL-10 levels in brain tissues in a dose-dependent manner (Supplementary Fig. S1 and Supplementary Fig. S1). In addition, the content of NO in serum and tissue was also detected, and NK could significantly reduce its level (Fig. 3C and Supplementary Fig. S1). Altogether, this observation suggested the promising potential of NK as an anti-inflammatory agent in tMCAO rats.

In the brain, microglia and astrocyte are the main sources of inflammation, so we examined the effect of NK on both cellular inflammation models. To examine NK's anti-inflammatory properties in microglia, we conducted an additional study to assess its impact on nuclear factor (NF)- $\kappa$ B activation induced by LPS in BV2 cells. As depicted in Figure 3D, LPS initiated the phosphorylation and degradation of inhibitor kappa B  $\alpha$  (I $\kappa$ B $\alpha$ ), both of which were alleviated in a concentration-dependent manner by NK. Correspondingly, there was a translocation of p65 to the nucleus (Fig. 3E), where it prompted the transcription of inducible nitric oxide synthase (iNOS) (Fig. 3F). Subsequently, this series of events led to elevated levels of inflammatory signaling molecules, NO (Fig. 3G), and proinflammatory cytokine, TNF- $\alpha$  (Fig. 3H). NK effectively restrained the NF- $\kappa$ B activation induced by LPS and the ensuing generation of proinflammatory factors within microglial cells. Similarly, in a model of astrocyte inflammation induced by LPS, we found that NK can reduce the release of NO and TNF- $\alpha$  in a concentration-dependent manner (Supplementary Fig. S1). These

observations underscored the anti-inflammatory impact of NK in microglia and astrocyte cells.

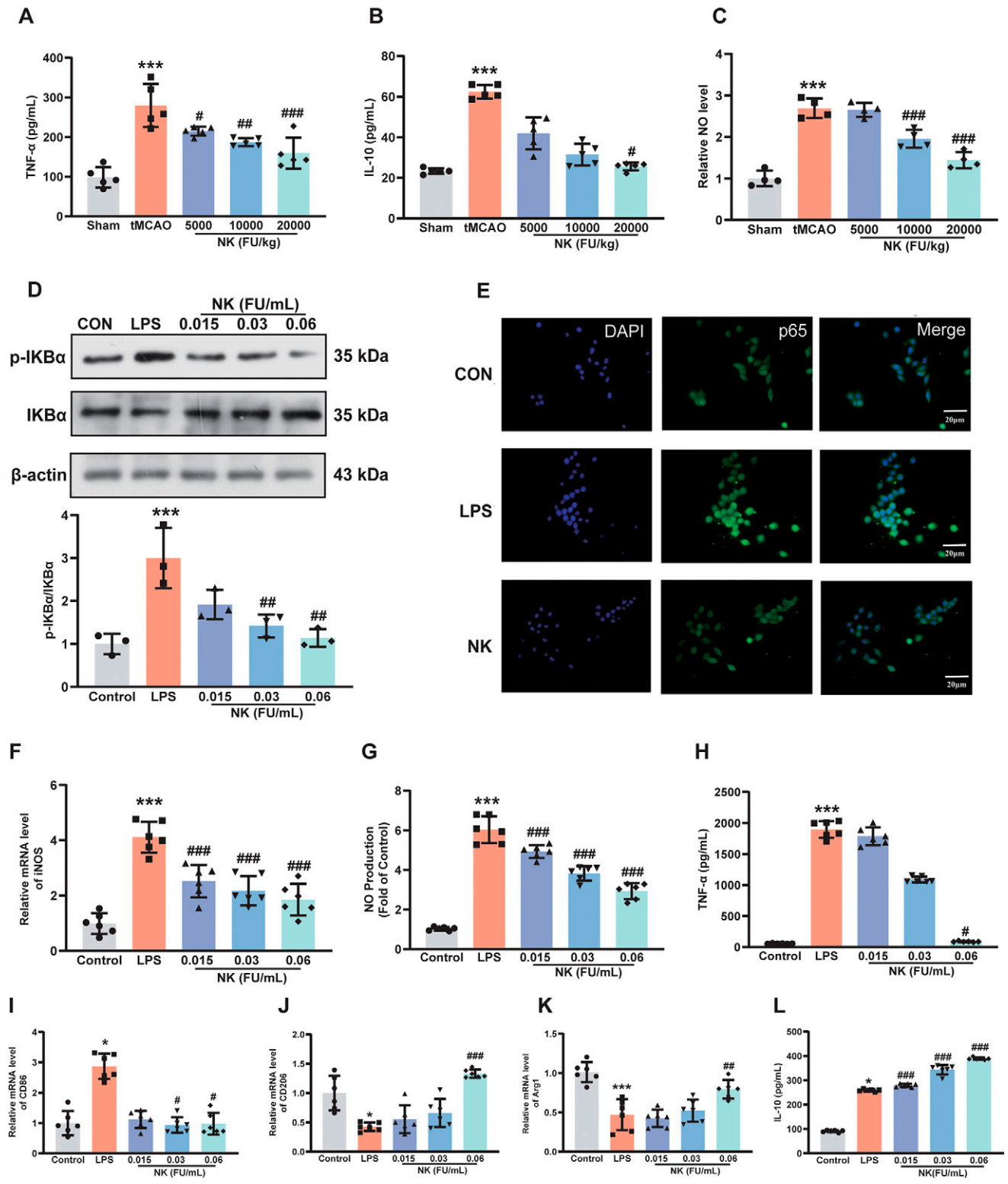
In addition to p65 translocation and proinflammatory release, LPS also activates microglia and induces changes in their phenotypes, specifically M1 and M2 polarization. To assess this, we further examined the makers associated with microglial polarization using qualitative polymerase chain reaction (qPCR). NK significantly suppressed the mRNA levels of M1 makers, such as iNOS and CD86, compared with those of the LPS-treated group (Fig. 3F and Fig. 3I). Conversely, the expression of M2 makers, including CD206 and Arg1, demonstrated an increase following administration of NK (Fig. 3J and Fig. 3K). Furthermore, there was a rise in the levels of the anti-inflammatory cytokine IL-10 following NK treatment (Fig. 3L), emphasizing the augmentation of microglial M2 polarization by NK. Taken together, these results suggested that the anti-inflammatory effect of NK was associated with shifts in microglial phenotypes.

To further evaluate the influence of NK on microglia polarization and activation in tMCAO rats, brain tissue was subjected to IBA1 staining, which served as a marker for microglia. We measured the effect of NK on microglial morphology by quantifying the number of microglial endpoints and process length per cell *via* the ImageJ analysis techniques. We showed that the process endpoints on microglia decreased after tMCAO, and NK can reverse these changes (Supplementary Fig. S1), signifying NK's effectively inhibition of microglial activation in tMCAO rats. In line with the observation that NK promoted M2 promotion in LPS-stimulated BV2 cells, NK suppressed the expression of the M1 surface markers CD86 and iNOS (Supplementary Fig. S1 and Supplementary Fig. S1), while simultaneously augmenting the expression of the M2 surface markers, CD206 and Arg1, following tMCAO (Supplementary Fig. S1 and Supplementary Fig. S1). These findings collectively indicated that NK held the potential to not only inhibit microglial activation but also promote M2 polarization, suggesting its significant anti-inflammatory impact in tMCAO-induced conditions.

#### *NK protected against LPS-induced BV2 microglia activation likely through serine protease activity*

Furthermore, a coculture system combining microglial cells and neurons was employed to investigate the potential protective effects of NK against neuronal cell death resulting

**FIG. 3. NK suppressed the proinflammatory cytokine release both in tMCAO rats and microglia.** Assessment of TNF- $\alpha$  and IL-10 levels were conducted through ELISA 24 h after the tMCAO procedure. (A–B) The concentrations of TNF- $\alpha$  and IL-10 in the serum of different experimental groups were measured. (C) The content of NO in the serum was measured by Griess reagent. \*\*\* $p$  < 0.001 vs. Sham group and # $p$  < 0.05, ## $p$  < 0.01, and ### $p$  < 0.001 vs. tMCAO group (n = 5). (D) Expression of I $\kappa$ B $\alpha$  and p-I $\kappa$ B $\alpha$  were assessed 24 h after LPS treatment. (E) Representative images of BV2 cells costained with antibodies against p65 (green) and DAPI (blue). Scale bar: 20  $\mu$ m. (F) The expression of iNOS was detected in LPS-treated BV2 microglial cells by qPCR. (G) The release of NO in the supernatants of BV2 cells detected by the Griess assay. The data were expressed as fold change of controls. (H) The concentration of TNF- $\alpha$  in cell supernatants was tested by ELISA. The mRNA expression levels of microglial polarization markers were measured, including (I) CD86, (J) CD206, and (K) Arg1 in BV2 cells stimulated by LPS. Data expressed as fold change of controls. (L) Concentrations of IL-10 in the cell supernatant was detected by ELISA. Results are expressed as means  $\pm$  SD from 6 independent experiments. Statistical analysis was performed with one-way ANOVA followed by Tukey. The graph B, H, I, and J was analyzed by the Kruskal–Wallis test followed by Dunn's post-test. \* $p$  < 0.05, \*\*\* $p$  < 0.001, vs. control; # $p$  < 0.05, ## $p$  < 0.01, ### $p$  < 0.001, versus LPS-stimulated cells. ELISA, enzyme-linked immunosorbent assay; LPS, lipopolysaccharides; I $\kappa$ B $\alpha$ , inhibitor kappa B  $\alpha$ ; TNF- $\alpha$ , tumor necrosis factor-alpha; IL, interleukin.



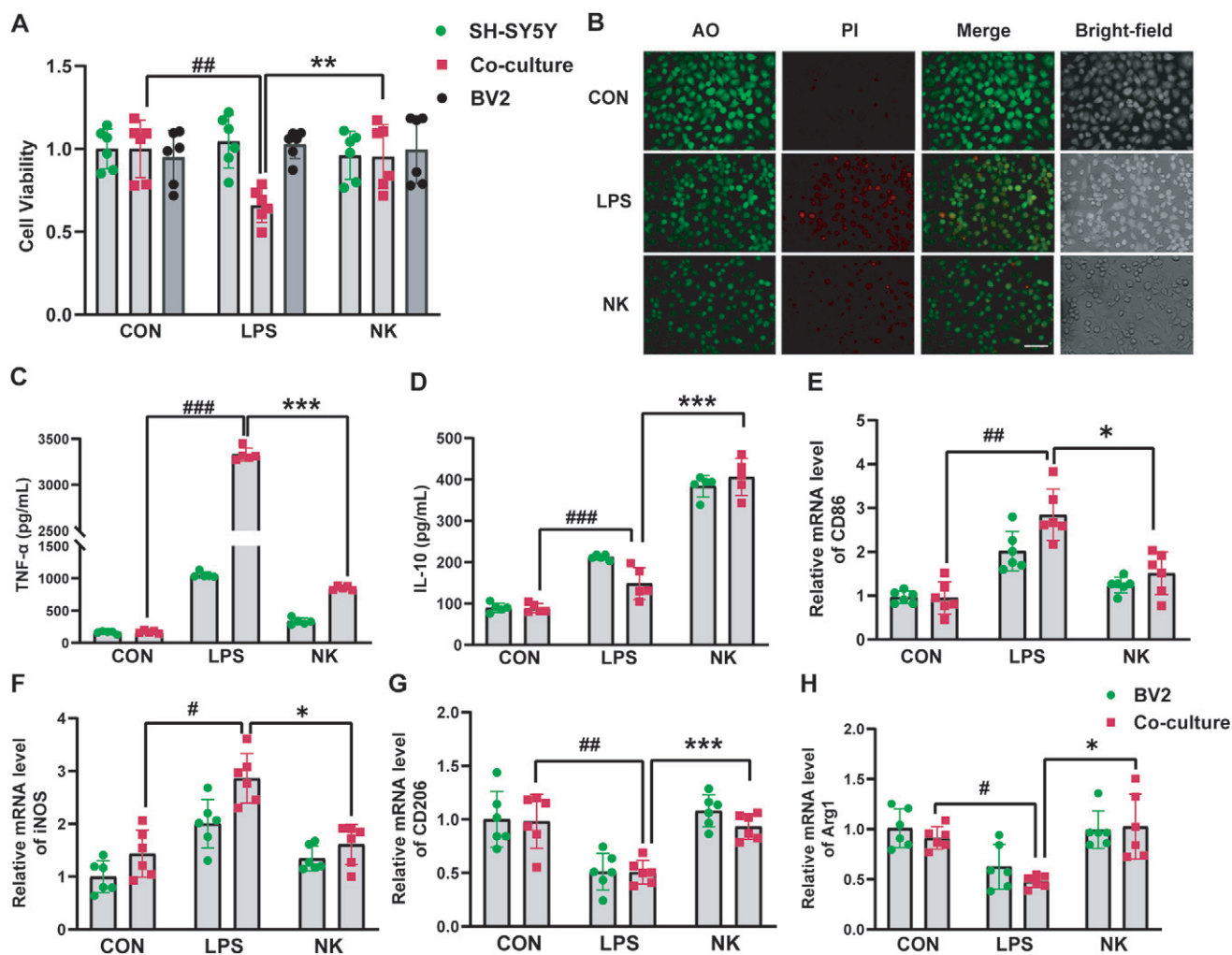


**FIG. 4. NK suppressed neuron death and modulated microglia polarization in the coculture system.**

(A) Quantitative analysis of cell viability detected by MTT assays. The coculture system consisted of SH-SY5Y cells and BV2 cells in a ratio of 3:1. Cells were pretreated with NK (0.06 FU/mL) for 2 h and then exposed to LPS (0.1  $\mu$ g/mL) for 24 h. Cell viability was measured by MTT after LPS exposure. (B) Representative images of fluorescence staining with PI (red) and AO (green). (C–D) Effect of NK on TNF- $\alpha$  and IL-10 release in BV2 cells alone or in a coculture system after being exposed to LPS (0.1  $\mu$ g/mL) for 24 h. (E–H) Quantitative analysis of inflammatory factors (E) CD86, (F) iNOS, (G) CD206, and (H) Arg1 detected by qPCR both in BV2 cells alone or coculture system. Data are shown as mean  $\pm$  SD ( $n = 6$ ). Statistical analysis was performed with one-way ANOVA followed by Tukey.  $^{##}p < 0.01$ ,  $^{###}p < 0.001$ , *versus* control of the coculture cells;  $^{*}p < 0.05$ ;  $^{**}p < 0.01$ ;  $^{***}p < 0.001$  vs. LPS-stimulated coculture cells. MTT, methyl thiazolyl tetrazolium; PI, propidium iodide; AO, acridine orange.

from microglial activation. As demonstrated in Figure 4, exposure to LPS induced noticeable cell death specifically in cocultured cells, while exerting no impact on individual cell types, as evidenced by both methyl thiazolyl tetrazolium (MTT) assay (Fig. 4A) and acridine orange/propidium iodide (AO/PI) staining (Fig. 4B). Pretreatment with NK substantially enhanced cell viability within the coculture system. NK treatment efficiently suppressed the release of TNF- $\alpha$  after LPS inducement (Fig. 4C), while concurrently elevating the level of IL-10 release (Fig. 4D), suggesting the phenotypic switch of the microglial cells. This was further supported by the evident upregulation of microglial M1 makers CD86 and iNOS (Fig. 4E and Fig. 4F), accompanied by a downregulation of the M2 markers CD206 and Arg1 (Fig. 4G and Fig. 4H) in the coculture system. Strikingly, NK reversed these alterations.

Similarly, we obtained comparable results in a coculture model of neurons and microglia, which are both from the mouse species (Supplementary Fig. S2). Therefore, NK showcased its potential for neuroprotection in SH-SY5Y cells and the promotion of M2 microglial polarization within the coculture system upon LPS stimulation.

Our previous data have established a connection between NK and its reliance on serine protease activity for toll-like receptor 4 (TLR4) degradation in RAW264.7 macrophages (Wu et al., 2020). Notably, NK also facilitated a time-dependent TLR4 proteolysis, which was concentration dependently protected by PMSF in BV2 cells (Fig. 5A). Considering TLR4's role as the central mediator in LPS-triggered activation of microglial inflammatory responses, we proceeded to investigate NK's impact on TLR4 levels in BV2

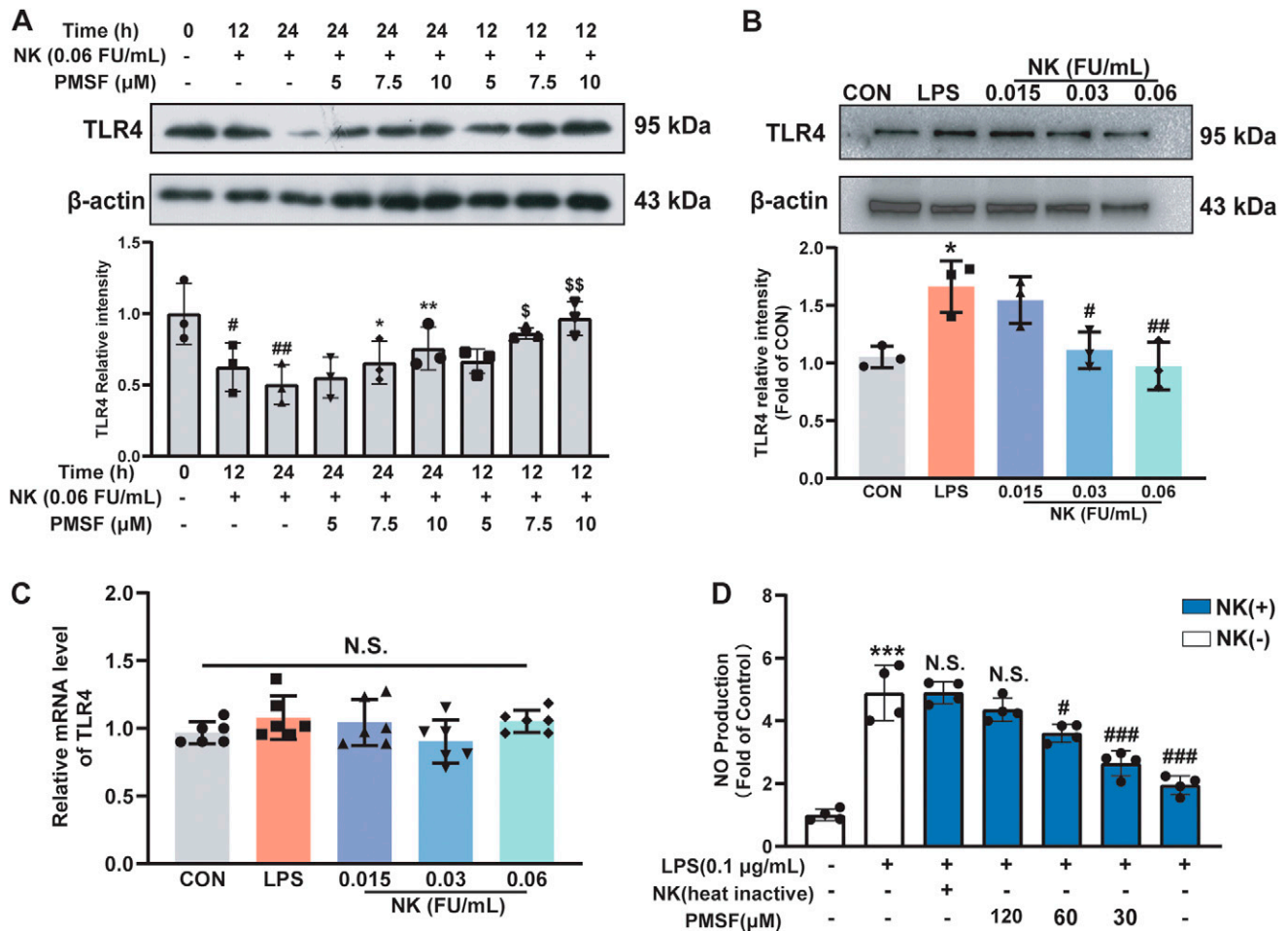


**FIG. 5. NK protected against LPS-mediated BV2 microglial activation likely through its serine protease activity.** (A) Effect of NK on TLR4 expression levels in BV2 cells. Cells were treated with NK (0.06 FU/mL) for indicated time points with or without PMSF pretreatment for 2 h. Western blot was performed with  $\beta$ -actin being the loading control. Results were quantified by densitometry. Data represented as means  $\pm$  SD ( $n = 3$ ). # $p < 0.05$ , ## $p < 0.01$  compared with 0 h; \* $p < 0.05$ , \*\* $p < 0.01$  compared with NK 24 h group; \$ $p < 0.05$ , \$\$ $p < 0.01$  compared with NK 12 h group. (B) Effect of NK on TLR4 levels in BV2 microglial cells following LPS stimulation. (C) Effect of NK on the mRNA level of TLR4 in LPS-treated BV2 microglial cells. (D) Effect of NK on LPS-induced NO release inhibited by heat-inactivated NK or indicated concentrations of PMSF in BV2 cells. Cells were preincubated with heat-inactivated NK or series concentrations of PMSF with NK (0.06 FU/mL) for 2 h before LPS stimulation. The medium was collected to detect NO production using the Griess assay 24 h following LPS. Results are expressed as means  $\pm$  SD from 3–6 independent experiments. Statistical analysis was performed with one-way ANOVA followed by Tukey. \* $p < 0.05$ , \*\*\* $p < 0.01$ , versus Control; # $p < 0.05$ , ## $p < 0.01$ , ### $p < 0.001$ , versus LPS-stimulated cells. TLR4, toll-like receptor 4; PMSF, phenylmethylsulfonyl fluoride.

microglial cells following LPS stimulation. As illustrated in Figure 5B, NK reduced TLR4 levels in response to LPS stimulation, without affecting its mRNA expression (Fig. 5C). In particular, in alignment with the impact of PMSF on LPS-induced TLR4 upregulation, PMSF also mitigated the protective effect of NK against LPS-mediated NO release in BV2 cells in a concentration-dependent manner (Fig. 5D), indicating that NK protected against LPS-mediated BV2 microglia activation likely through its serine protease activity. This was further supported by the observation that the heat-inactive NK failed to exert any protective effects (Fig. 5D). In summary, these findings collectively demonstrated that NK restrained LPS-induced inflammation and polarization in BV2 microglia

cells, with a robust link to its serine protease activity, which was likely achieved through promoting TLR4 degradation.

#### *NK effectively mitigated oxidative stress induced by tMCAO and OGD/R*

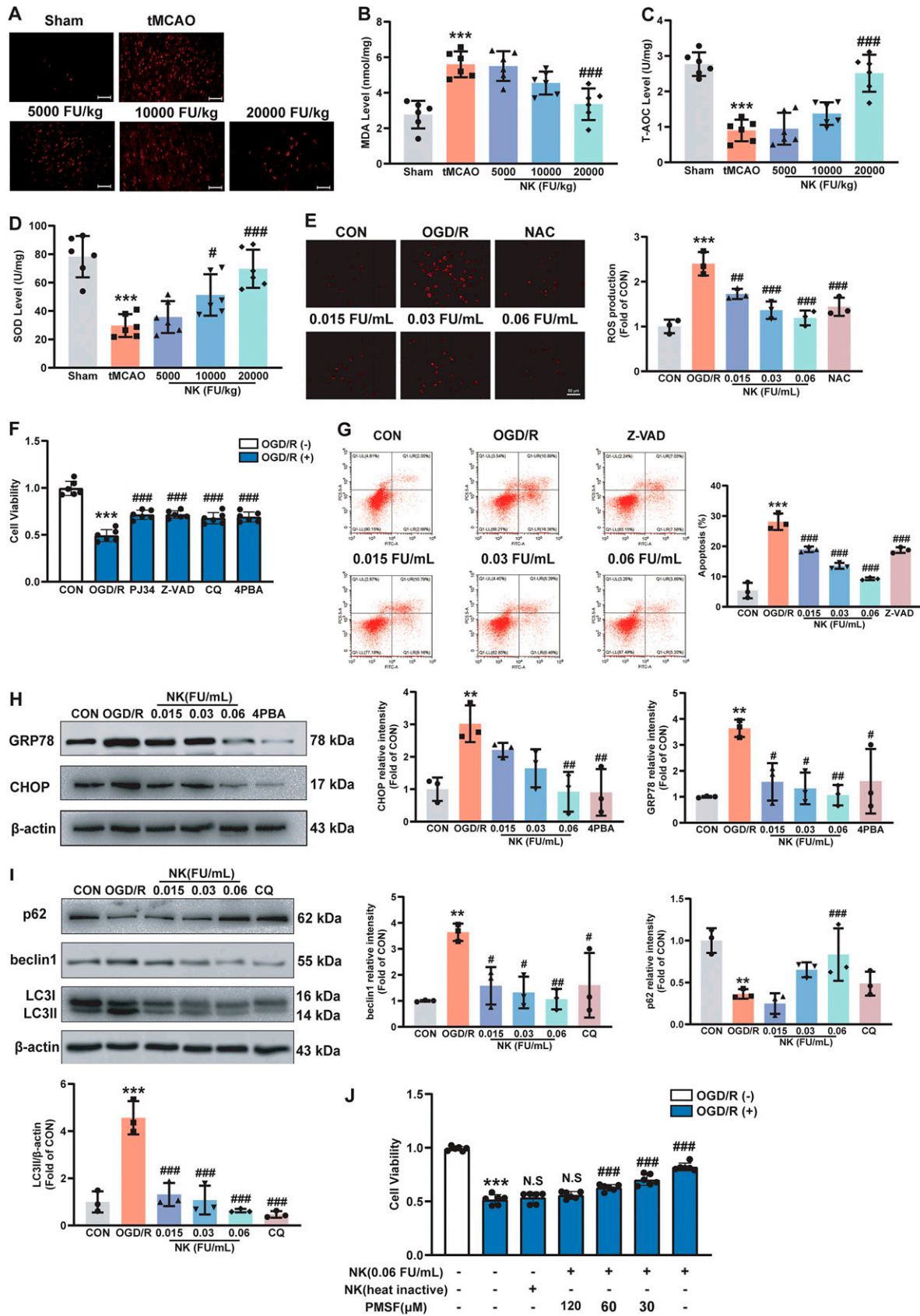
Oxidative stress is a critical player in the pathogenesis of cerebral ischemia/reperfusion injury. As evidenced by dihydroergotamine (DHE) staining in Figure 6A, tMCAO resulted in a significant upsurge in ROS production within brain tissue, which was alleviated by NK administration in a dose-dependent pattern. Furthermore, the activity of malondialdehyde (MDA), a recognized marker of oxidative stress,

substantially increased in the cortex of tMCAO-operated rats, underlining the oxidative stress occurrence. NK administration dose dependently curbed MDA generation (Fig. 6B). In addition, both total antioxidant capacity (T-AOC) and superoxide dismutase (SOD) levels exhibited a decline in response to cerebral ischemia/reperfusion injury. NK treatment bolstered the activity of these antioxidative factors in brain tissue (Fig. 6C and Fig. 6D). Concurrently, we accessed the relevant oxidative stress makers in the serum. As shown in Supplementary Figure S3, the concentration of MDA in serum escalated after tMCAO induction, while NK treatment demonstrated a capacity to attenuate MDA content. Furthermore, NK exhibited a dose-dependent elevation in T-AOC and SOD levels in serum, mirroring observations in brain tissue (Supplementary Fig. S3 and Supplementary Fig. S3). Collectively, these findings presented compelling evidence that NK proficiently ameliorated oxidative damage in the context of cerebral ischemia/reperfusion injury. Building upon the evidence of NK's potential to attenuate oxidative stress in the tMCAO model, the oxygen–glucose deprivation/reperfusion (OGD/R) model was employed to further delve into its neuroprotective mechanisms. As shown in Figure 6E, the DHE fluorescent intensity was lower in NK-treated cells compared with those subjected to OGD/R injury without NK administration. This finding highlighted NK's role in substantially reducing the intracellular ROS levels induced by OGD/R damage. Moreover, cell viability data corroborated NK's efficacy in enhancing neuron survival under OGD/R conditions, underscoring its protective effect against OGD/R injury (Supplementary Fig. S3). To unravel the multifaceted mechanisms underlying cell death triggered by OGD/R, a comprehensive panel of cell death inhibitors targeting apoptosis (Z-VAD-FMK), autophagy (CQ), PARP-dependent cell death (PJ34), as well as the ER stress (4PBA) were employed. As revealed in Figure 6F, the administration of these inhibitors significantly mitigated OGD/R-induced cell death, pointing toward the involvement of these pathophysiological cascades in OGD/R. Consequently, the study proceeded to investigate the effect of NK across various forms of cell death induced by OGD/R. Primarily, attention was focused on NK's impact on apoptosis. Flow cytometry results demonstrated that NK effectively suppressed OGD/R-induced neuronal death in a concentration-dependent

manner (Fig. 6G). Moreover, protein levels of apoptosis-related factors, including caspase3, cleaved caspase3, Bcl2-associated X (Bax), and B-cell lymphoma-2 (Bcl2) were assessed 24 h post-OGD/R treatment (Supplementary Fig. S3). OGD/R-treated neurons exhibited elevated protein levels of Bax and cleaved caspase3, accompanied by decreased levels of Bcl2 when compared with untreated SH-SY5Y cells. NK intervention counteracted these alterations induced by OGD/R, leading to reduce Bax and cleaved caspase3 levels, and to increase Bcl2 levels. Furthermore, our exploration extended to the analysis of poly (ADP-ribose) (PAR) protein expression levels, solidifying NK's capacity to effectively counter PAR polymerase (PARP) overactivation (Supplementary Fig. S3). We also probed NK's impact on ER stress. Notably, NK displayed a concentration-dependent reduction in the protein levels of glucose-regulated protein 78 (GRP78) and C/EBP homologous protein (CHOP), both recognized as critical markers of ER stress. This indicated NK's substantial ability to attenuate ER stress triggered by OGD/R (Fig. 6H). Additionally, the assessment of key proteins in the autophagy pathway, including p62, Beclin1, and LC3, revealed that NK mitigated the process of autophagy (Fig. 6I). This comprehensive array of results collectively underscored NK's efficacy in inhibiting apoptosis, mitigating ER stress, suppressing autophagy, and addressing PARP overactivation induced by OGD/R.

Notably, analogous to our observations in the LPS experiments, NK's protective mechanism in the OGD/R model was also attributed to its serine endopeptidase activity, as evidenced by the fact that heat-inactivated NK failed to exert protective effects against OGD/R-induced neuronal death. Furthermore, the effectiveness of NK protection exhibited a concentration-dependent decrease when exposed to increasing concentrations of PMSF (Fig. 6J). NK demonstrated a concentration-dependent counteraction of the heightened TLR4 levels induced by OGD/R (Supplementary Fig. S3). This observation further bolstered the established link between NK's effect and TLR4 from our previous LPS model (Fig. 5). To delve deeper into this relationship, the TLR4 inhibitor Resatorvid (TAK242) was employed. As depicted in Supplementary Fig. S3, TAK242 also mitigated the escalated TLR4 levels induced by OGD/R. TAK242 also

**FIG. 6. NK mitigated tMCAO and OGD/R-induced oxidative stress in rats.** (A) Representative images stained with DHE (red) of the cortex area in the infarcted lateral hemisphere. Scale bars: 100  $\mu$ m. Quantitative analysis of DHE-positive cells counted by ImageJ. (B–D) The levels of MDA, T-AOC, and SOD in the tissue of the infarcted lateral hemisphere cortex were assessed by relevant test kits.  $^{***}p < 0.001$ , versus Sham;  $^{\#}p < 0.05$ ,  $^{##}p < 0.01$ ,  $^{###}p < 0.001$  versus tMCAO ( $n = 6$ ). (E) Effect of NK on OGD/R-induced ROS generation in SH-SY5Y cells. Cells were treated with NK (0.015, 0.03, 0.06 FU/mL) or NAC (1 mM) for 2 h before OGD treatment. After 4 h of oxygen–glucose deprivation, cells were cultured in regular medium for an additional 24 h. (F) Cells were pretreated with Z-VAD-FMK (10  $\mu$ M), CQ (10  $\mu$ M), PJ34 (2  $\mu$ M), or 4PBA (40  $\mu$ M) for 4 h before OGD/R treatment for 4 h. Cell viability was tested by MTT assay. (G) Effect of NK on OGD/R-induced apoptosis in SH-SY5Y cells. Cell apoptosis was detected via the Annexin V/PI Double Staining Kit with flow cytometry. (H) Effect of NK on OGD/R-induced ER stress in SH-SY5Y cells according to the protein expression of GRP78 and CHOP by Western blotting. (I) Expression of autophagy proteins were assessed 24 h after OGD/R. Values were expressed as means  $\pm$  SD ( $n = 3$ –6). (J) MTT assay was conducted to detect the protection effect of TAK242 on OGD/R-induced cell death. Values were expressed as means  $\pm$  SD ( $n = 6$ ). Statistical analysis was performed with one-way ANOVA followed by Tukey.  $^{**}p < 0.01$ ,  $^{***}p < 0.001$ , versus CON;  $^{\#}p < 0.05$ ,  $^{##}p < 0.01$ ,  $^{###}p < 0.001$ , versus OGD/R-treated cell. DHE, dihydroergotamine; MDA, malondialdehyde; T-AOC, total antioxidant capacity; SOD, superoxide dismutase; PAR, poly (ADP-ribose); ROS, reactive oxygen species; NAC, N-Acetylcysteine; TAK242, Resatorvid.



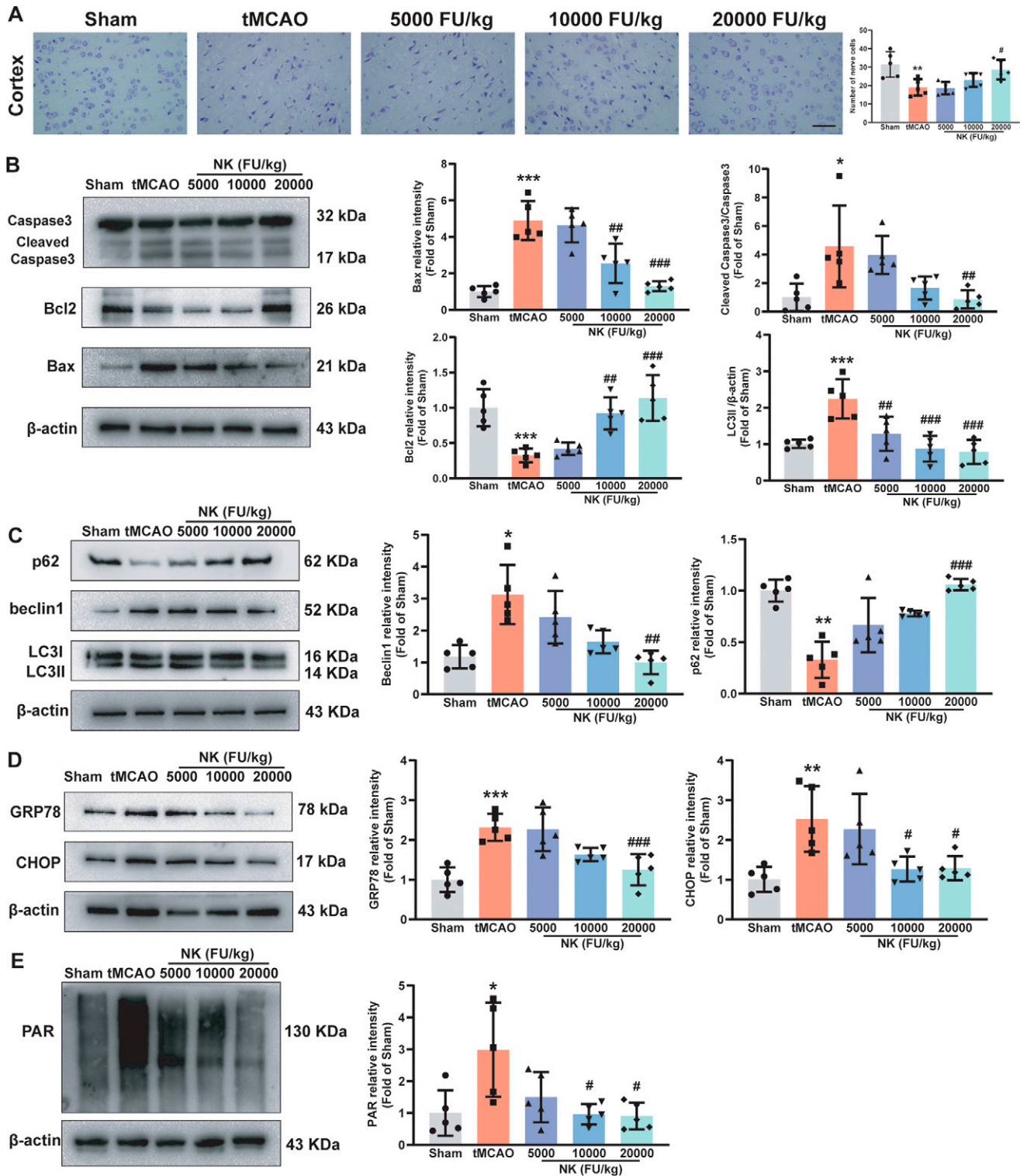


**FIG. 7. NK suppressed apoptosis, autophagy, and PARP overactivation in neuronal cells following tMCAO.** (A) Neuronal cell survival in the infarcted lateral hemisphere cortex was determined by Nissl staining. Scale bars = 50  $\mu$ m. (B) The protein expression of caspase3, cleaved caspase3, Bcl2, and Bax were conducted by Western blot in the infarcted lateral hemisphere cortex. (C) Western blot analysis was performed to evaluate the protein levels of p62, beclin1, and LC3. (D) Quantitative analysis for the relative protein levels of GRP78 and CHOP. (E) Western blot analysis was employed to determine the protein level of PAR. Values were expressed as means  $\pm$  SD. Statistical analysis was performed with one-way ANOVA followed by Tukey. \* $p$  < 0.05, \*\* $p$  < 0.01, \*\*\* $p$  < 0.001 versus Sham; # $p$  < 0.05, ## $p$  < 0.01, ### $p$  < 0.001, versus tMCAO ( $n$  = 5). PAR, poly (ADP-ribose).

exhibited a concentration-dependent protective effect against OGD/R-induced neuronal injury (Supplementary Fig. S3). Overall, these results indicated that NK's protective effects were correlated with its serine endopeptidase activity, highlighting NK's analogous role to a TLR4 inhibitor in the OGD/R model.

#### *NK exerted multifaceted neuroprotection against cell death pathways following tMCAO*

To unravel the potential neuroprotective mechanisms of NK in the context of cerebral ischemia, comprehensive assessments were performed using brain sections subjected to Nissl staining, as well as molecular analyses targeting various cell death pathways. As shown in Figure 7A, Nissl staining revealed a noteworthy reduction in neuronal death within the cortex regions of the brain following tMCAO when treated with NK. This observation highlighted NK's potential to alleviate neuronal loss caused by cerebral ischemia, underlining its neuroprotective properties. Moreover, Western blot analysis offered further insights into NK's mechanisms of action. Similar to observations in the OGD/R model, NK treatment augmented the protein level of Bcl2 and decreased Bax, while concomitantly decreasing the expression of cleaved caspase3 compared with the tMCAO group (Fig. 7B). However, NK demonstrated a dose-dependent inhibitory effect on this upregulation, delineating its potential to mitigate autophagy triggered by tMCAO (Fig. 7C). As evidenced by the results presented in Figure 7D, key factors of ER stress, namely CHOP and GRP78, exhibited upregulation

following tMCAO. Furthermore, NK exhibited suppression of the PARP overactivation (Fig. 7E). These combined results provided robust evidence that NK held the potential to inhibit apoptosis, autophagy, ER stress, and PARP overactivation, suggesting a promising therapeutic role for NK in addressing the pathological process associated with tMCAO.

#### *NK effectively reduced the levels of thrombin, FIB, and PAI-1 in tMCAO rats*

We have previously reported on NK's comprehensive antithrombus strategy, which involved disrupting the detrimental cycle linking inflammation, oxidative stress, and thrombus (Wu et al., 2020). It was noteworthy that the consistent observations across multiple models indicated that NK's protective effect heavily relied on its enzymatic activity. With this understanding, we aimed to gain a deeper insight by exploring its impact on coagulation-related factors in the serum of tMCAO rats. Impressively, our observations highlighted the exceptional efficacy of NK in mitigating the elevated levels of its substrates, including thrombin (Fig. 8A), plasminogen activator inhibitor-1 (PAI-1) (Fig. 8B), and fibrinogen (FIB) (Fig. 8C), while not affecting tissue plasminogen activator (tPA) levels (Fig. 8D) in the tMCAO rats. These findings provided evidence that NK efficiently inhibited coagulation, likely due to its enzyme activity that allowed it to substantially decrease the levels of its substrates within the tMCAO model.

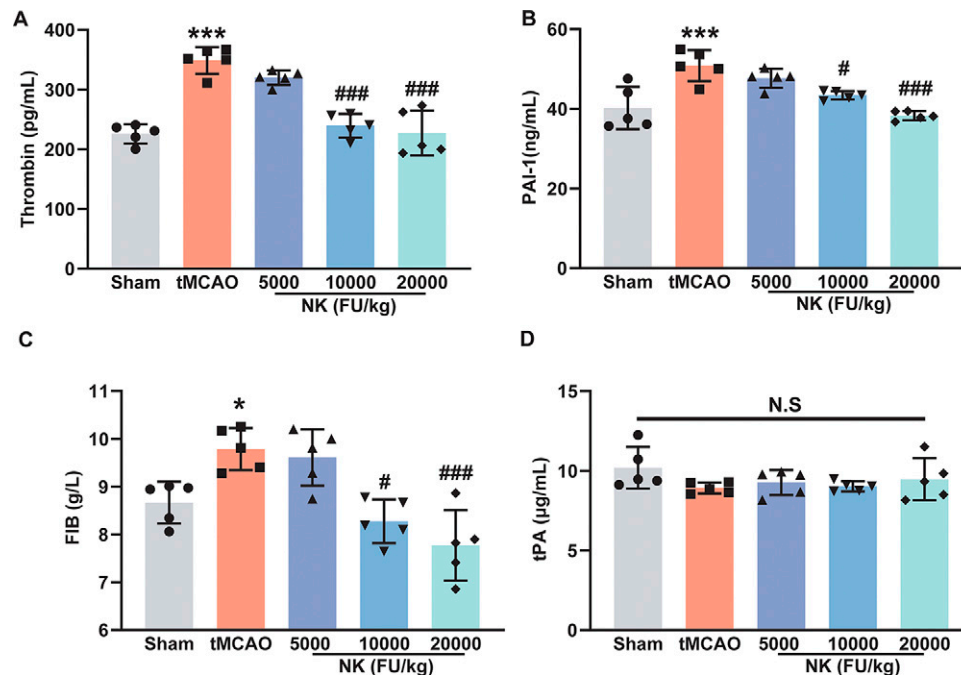


**FIG. 8.** Effect of NK on serum levels of thrombin, PAI-1, FIB, and tPA in tMCAO rats. Serum concentrations of thrombin (A) and PAI-1 (B) were detected *via* ELISA. (C–D) The levels of FIB (C) and tPA (D) in the rat serum were measured by ELISA. Data were expressed as mean  $\pm$  SD. Statistical analysis was performed with one-way ANOVA followed by Tukey. \* $p < 0.05$ , \*\*\* $p < 0.001$  vs. Sham; # $p < 0.05$ , ### $p < 0.001$ , versus tMCAO ( $n = 5$ ). PAI-1, plasminogen activator inhibitor-1; FIB, fibrinogen; tPA, tissue plasminogen activator.

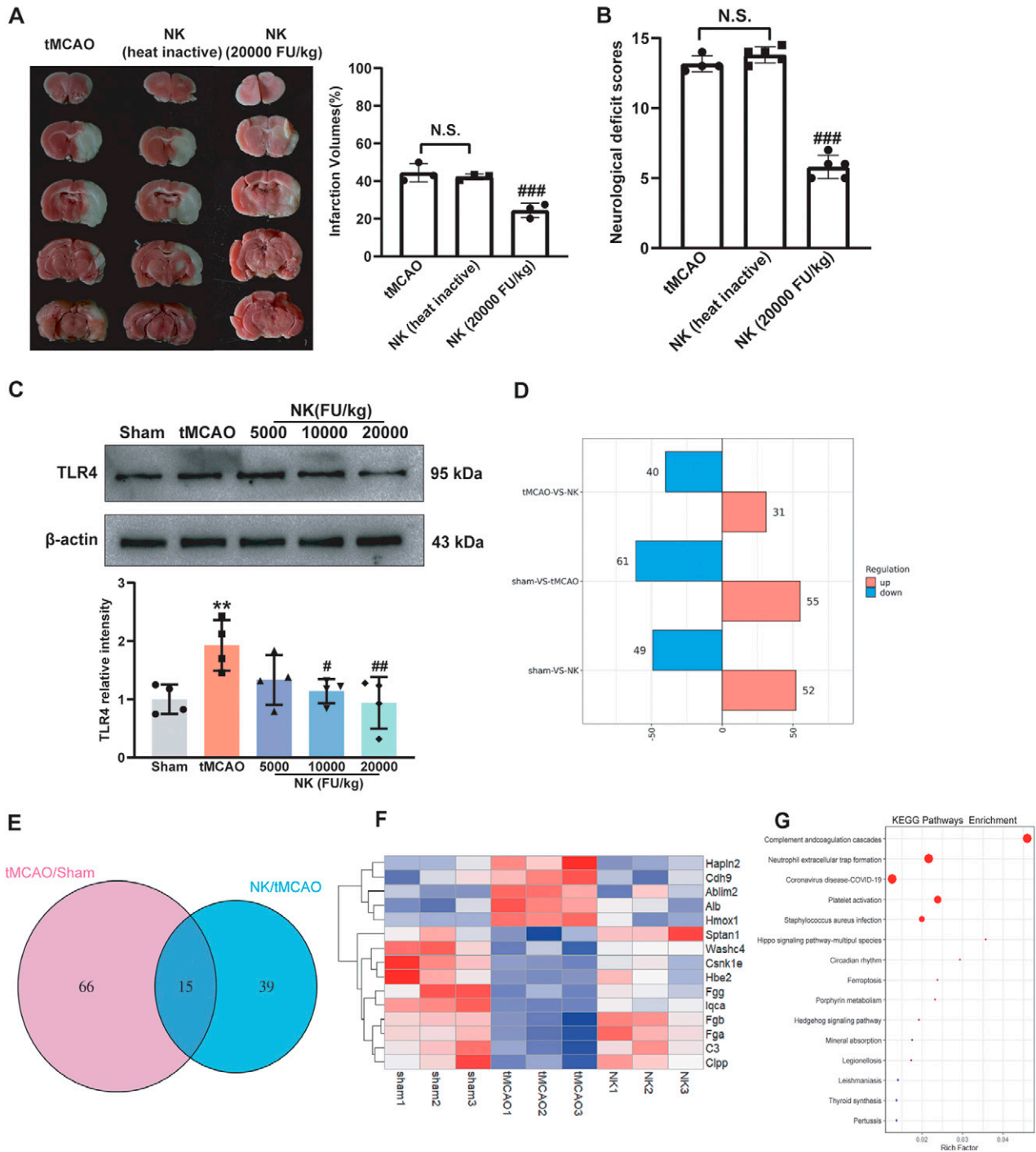


**FIG. 9. The protective effect of NK against tMCAO was dependent on its enzymatic activity. (A)** The impact of heat-inactive NK on tMCAO rats. The percentage of the relative infarct volume was calculated by TTC staining. **(B)** Neurological function was assessed with the mNSS. **(C)** Effect of NK on tMCAO-induced TLR4 expression in rats. Data were shown as mean  $\pm$  SD ( $n = 3-4$ ). Statistical analysis was performed with one-way ANOVA followed by Tukey.  $**p < 0.01$  versus Sham;  $\#p < 0.05$ ,  $###p < 0.001$ ,  $####p < 0.0001$ , vs. tMCAO ( $n = 3-4$ ). **(D)** The number of significant altered proteins in each experimental group. **(E)** Venn diagram showing the common DEPs in the comparison of tMCAO versus Sham and NK versus tMCAO. **(F)** The heat map visualizing the expression changes of overlapped DEPs. **(G)** The KEGG enrichment pathway bar plot of the overlapped DEPs ( $n = 3$ ). KEGG, Kyoto Encyclopedia of Genes and Genomes; DEPs, differential expressed proteins.

### *The protective effect of NK against tMCAO was dependent on its enzymatic activity*

NK, acknowledged as a serine protease, has previously been associated with its serine protease activity. Encouragingly, our observations revealed that when heat inactivated, NK was unable to confer any protective effects against tMCAO injury (Fig. 9A). At the same time, it failed to show any influence on the motor function of the animals (Fig. 9B). Additionally, we noted a significant increase in the expression level of TLR4 on the ipsilateral side of the brain in tMCAO animals in the sham group. Similar to the findings in the LPS-induced microglia activation model and OGD/R model, this increase was alleviated by NK treatment (Fig. 9C). These findings indicated that the protective properties of NK *in vivo* were closely connected to its enzymatic activity.

To assess the impact of NK on brain protein alterations in tMCAO rats, we conducted data-dependent acquisition (DIA) quantitative proteomics on cerebral ischemic brain tissues. As shown in Figure 9D, a total of 116 proteins exhibited differential expressions in response to tMCAO when compared with the sham group. Following NK administration, a specific subset of 71 proteins demonstrated considerable changes in comparison to the tMCAO group (Fig. 9D). This emphasized NK's potential regulatory role in regulating protein expression patterns during tMCAO-induced injury. Furthermore, a Venn diagram analysis revealed that 15 differential expressed proteins (DEPs) were coexpressed both in the tMCAO/sham and NK/tMCAO comparisons (Fig. 9E). Among these, 5 genes were downregulated induced by NK, including Hapln2, Cdh9, Ablim2, Alb, and Hmox1, while 10 proteins demonstrated increased expression (Fig. 9F). To gain insight into the functional changes, Kyoto Encyclopedia of Genes and Genomes (KEGG) pathway annotation was carried out. As illustrated in Figure 9G, these DEPs were primarily associated with complement and coagulation cascades, neutrophil extracellular trap formation, and platelet activation. This confirmed NK's effectiveness in protecting against tMCAO injury by regulating coagulation and inflammation processes.

### Discussion

IS is a devastating disease known for its severe consequences and high mortality rates. It involves intricate pathophysiological processes, including inflammation, oxidative stress, coagulation, and neuronal death. Current treatment strategies for IS primarily focused on either of the two pivotal approaches: the administration of thrombolytic drugs, such as rtPA thrombolytics, and the use of neuroprotective drugs (Herpich and Rincon, 2020). However, despite these efforts, the clinical efficacy of these treatments remains limited. Thrombolytic drugs are hindered by a narrow treatment window, while neuroprotective drugs face challenges in achieving desirable outcomes (Richards and Cramer, 2023). Consequently, the development of therapeutic agents with dual capabilities in both thrombolysis and neuroprotection holds great promise and presents unique advantages for the future of IS treatment. Notably, NK is renowned for its extraordinary antithrombotic properties, particularly its efficacy in dissolving aged clots (Wu et al., 2019a). Especially, our previous study uncovered the comprehensive antithrombus

strategy of NK by breaking the vicious cycle among inflammation, oxidative stress, and thrombosis (Wu et al., 2020). In particular, a study recently revealed a robust neuroprotective effect of NK in ameliorating pMCAO-induced damage *via* promoting neuronal regeneration (Wu et al., 2023). These findings informed the multifaceted potential of NK as a promising agent in both thrombolysis and neuroprotection. We further explored its neuroprotective effects and mechanisms after confirming its impressive protective effect on tMCAO. In this study, we found that NK could exert neuroprotective effects in a variety of models *in vitro* and *in vivo*, including the tMCAO model, the microglia inflammation model and neuronal OGD/R model. NK exhibited remarkable efficacy in ameliorating infarct volume and improving sensorimotor and motor function in rats subjected to tMCAO. Moreover, NK demonstrated the ability to suppress proinflammatory mediators while concurrently promoting anti-inflammatory factors' expression in LPS-stimulated BV2 cells and tMCAO rats, indicative of a shift from the M1 to the M2 phenotype in microglia. The neuroprotective effects of NK were evident through its inhibition of various neuronal death pathways in models, as demonstrated in models such as OGD/R and tMCAO. Additionally, NK displayed substantial antioxidant properties by effectively inhibiting ROS production and augmenting the expression of antioxidant enzymes. Furthermore, NK exhibited noteworthy anticoagulant activity following tMCAO, collectively indicating its capacity to effectively disrupt the detrimental cycle encompassing oxidative stress, inflammation, and coagulation associated with tMCAO in rats (Fig. 1).

Studies have shown that inflammation is an important pathogenic factor of many thrombotic diseases such as IS. The phenomenon of neuroinflammation has significant implications for the pathophysiology of various neurological and neurodegenerative disorders (Rajan et al., 2019). Among the cells involved, microglia play a prominent role in post-injury inflammation, exerting a substantial influence on disease onset, progression, and neurological outcomes following acute brain injury (Poh et al., 2019). Consequently, precise regulation of neuroinflammation has emerged as a promising therapeutic avenue for stroke (Li and Barres, 2018). Our results revealed that NK effectively mitigated the release of inflammatory cytokines and suppressed the changes in microglial phenotype induced by both tMCAO and LPS. Notably, previous *in vivo* and *in vitro* investigations have demonstrated that modulating microglial polarization from an M1 to a neuroprotective M2 phenotype within IS during the early phase can confer protection against cerebral ischemia-reperfusion (I/R) injury (Kanazawa et al., 2017). Remarkably, activation of the NF- $\kappa$ B signaling pathway plays a pivotal role in regulating the proinflammatory M1 activation state in microglia (Aslanidis et al., 2015). Expanding upon these important findings, our study provided compelling evidence that NK prominently restrained microglial activation and facilitated their polarization toward the neuroprotective M2 phenotype both *in vitro* and *in vivo*. In addition, our study demonstrated the effective suppression of LPS-induced NF- $\kappa$ B p65 activation and consequential reduction of proinflammatory mediator production in microglial cells mediated by NK. In addition to the inflammation

factors, NK can reduce the release of NO, the important signal molecule in the immune response. NO led to the hypothesis that peroxynitrite, formed by the reaction between NO and a superoxide anion, might be responsible for the cellular damage in neurodegenerative disorders (Calabrese et al., 2007).

Furthermore, it should be acknowledged that our study, similar to a majority of other investigations, employed a binary M1/M2 polarization paradigm (Wu et al., 2021). However, there is an increasing recognition that the M1/M2 polarization concept oversimplifies the complex *in vivo* scenario and may not adequately capture the diverse polarized states exhibited by microglia in their native environment (Goldmann et al., 2013). In fact, accumulating evidence suggests that microglia display intricate and mixed phenotypes, thereby challenging the simplistic M1/M2 dichotomy as insufficient for defining microglial/macrophage polarization states and subsequent inflammatory profiles in cerebral ischemia–reperfusion (I/R) injury. Emerging research has convincingly demonstrated that microglial phenotypes after cerebral I/R injury extend beyond the classical M1/M2 categories. Despite these critical considerations, differentiating between M1 and M2 phenotypes may still offer important insights into understanding the role of microglia in the context of cerebral I/R injury (Ransohoff, 2016).

It is well known that excessive microglial activation, especially the M1 microglia, leads to expansion of neural damage and deterioration of neurological outcomes (Rao et al., 2021). The activated microglial can induce the neurons death, which aggravated the release of inflammatory factors and polarization in return (Bredesen et al., 2006; Nam et al., 2013). Our data also indicated that there is a feedback loop in the microglia and neuron, and NK can inhibit the production of inflammatory factors by LPS-induced microglial cells that can damage neurons. The demise of neurons is a critical factor contributing to the deleterious consequences of IS. Extensive reports have emphasized that neuronal death in the brain initiates within 24 h following the onset of IS, resulting from compromised nerve conduction (Yamaguchi and Miura, 2015). Overwhelming evidence supports the involvement of various death pathways in the pathologies of IS (Tuo et al., 2022). In this study, we demonstrated the effectiveness of inhibiting apoptosis, autophagy, ER stress, and PARP-dependent processed processes in suppressing neuronal cell death. Recent investigations have emphasized the crucial role of ER stress in neurodegeneration (Mancuso et al., 2008). During ischemia, energy depletion and calcium homeostasis disruption can trigger the accumulation of misfolded proteins within the ER lumen, which subsequently activates the unfolded protein response (UPR) (Lin et al., 2018). UPR activation serves to restore homeostasis and normalize ER function; if the damage is severe, it may culminate in cell death. Notably, CHOP, a transcription factor upregulated during ER stress, actively participates in ER-mediated apoptosis (Li et al., 2020). Our study reveals that NK downregulates the protein expression of CHOP and GRP78, following ischemia/reperfusion in rat brains and OGD/R-treated SH-SY5Y. Some studies suggested the vitagene network, comprising stress-responsive genes involved

in cellular defense mechanisms against oxidative stress, has garnered significant attention in recent research (Calabrese et al., 2010). These studies highlight the pivotal role of vitagene in maintaining cellular homeostasis and protecting against oxidative damage, particularly in the context of neurodegenerative diseases (Calabrese et al., 2016; Mancuso et al., 2008). Furthermore, emerging evidence suggests that nutritional interventions, such as mushroom-derived compounds, can modulate the vitagene network, offering potential therapeutic benefits (Concetta Scuto et al., 2019; D'Amico et al., 2021). Incorporating these findings into our discussion underscores the importance of understanding the vitagene-mediated mechanisms underlying neuroprotection and the potential of dietary interventions in promoting cellular resilience against oxidative stress-induced neurodegeneration. Collectively, these findings highlight the ability of NK to effectively suppress pivotal mediators implicated in ER stress and apoptosis under pathological conditions associated with I/R injury.

Additionally, we reckoned that PARP-dependent cell death also contributed to the neuronal death process. When IS occurred, numerous DNA strands are damaged and PARP activity reaches high levels due to the lack of energy. This heightened activity can induce programmed cell death (Koehler et al., 2021). Consistently, our findings revealed increased production of PAR in both the OGD/R and tMCAO models. Notably, pretreatment with NK effectively mitigated the elevation of PAR protein levels. Furthermore, accumulating evidence suggests a close association between neuronal death and autophagy (Wang et al., 2021). It is believed that following IS, autophagy in neurons exerts detrimental effects to the brain. Consistent with these observations, the autophagy inhibitor 3-methyladenine was found to suppress the increased neuronal death in both primary cortical neurons and SH-SY5Y neuronal cells exposed to OGD/R (Guo et al., 2021, Wang et al., 2022b). Our data provided evidence that NK exerted the protective effect by suppressing the autophagy after tMCAO. However, it should be noted that conflicting results have been reported regarding the involvement of enhanced autophagy in the neuroprotection effect (Wang et al., 2014). Several explanations may account for this discrepancy observed across different studies, including the utilization of diverse animal models such as the tMCAO model or the four-vessel occlusion model, which could influence the outcomes. Moreover, researchers have highlighted the importance of controlling physiological variables that modulate the severity of ischemia, including the degree of blood flow blockade, to ensure the acquisition of accurate and reliable data (Xu and Pan, 2013).

IS refers to the temporary or permanent interruption of blood supply to the cerebral vasculature, and the dissolving thrombus is the main clinical implication (Onose et al., 2022). While pharmacological thrombolysis primarily targets the thrombus itself, conventional thrombolytic drugs often exhibit limitations in terms of a narrow therapeutic time window and suboptimal efficacy. Notably, NK demonstrates potent thrombolytic effects, particularly against aged blood clots. Intriguingly, our investigation revealed a remarkable inhibitory effect of NK administration on coagulation in rats subjected to tMCAO, as evidenced by reduced

levels of thrombin, PAI-1, and FIB measured using ELISA. These findings are consistent with our previous studies conducted in animal models of AKI (Wu et al., 2020). Previous research has indicated that thrombin and FIB serve as hydrolytic substrates for NK, leading us to hypothesize that the protective effect of NK against IS may be attributed to its serine endopeptidase activity.

Based on the above results, we speculated that the mechanism of NK was closely linked to its serine endopeptidase. In our previous study, NK was found to exert an anti-inflammatory effect by degrading TLR4 expression levels in RAW264.7 cells. The present study further corroborates these findings, indicating that NK exerts a protective effect by degrading the expression of TLR4 protein in BV2 cells, without affecting its mRNA level. The Toll-like receptor (TLR) family plays a crucial role in the innate immune response, recognizing a variety of pathogen- and danger-associated molecular patterns to initiate inflammatory signaling cascades. While much attention has been focused on the canonical activation of TLRs by ligand binding, emerging evidence suggests that proteolytic processing also contributes to the regulation of TLR signaling pathways (Barton and Kagan, 2009). In particular, recent studies have shed light on the proteolytic regulation of TLR9, TLR7, and other TLRs, demonstrating that proteolysis can modulate its activation and downstream signaling (de Zoete et al., 2011; Ewald et al., 2008). In the context of IS, neuroinflammation drive by TLR's activation has been implicated in exacerbating tissue damage and contributing to poor outcomes (Zabel and Kirsch, 2013). TLR4, predominantly expressed in microglia, serves as a critical mediator of inflammation responses. Elevated TLR4 protein levels have been associated with an unfavorable prognosis for IS (Caso et al., 2007). Furthermore, TLR4 has been recognized as damage-related molecules, such as LPS (Tang et al., 2020). Our results demonstrated a time-dependent reduction in TLR4 levels in BV2 cells following NK incubation, which was concentration dependently abrogated by PMSF, a potent serine protease inhibitor. Strikingly, PMSF almost completely restored TLR4 levels, strongly indicating that downregulation of TLR4 expression is mainly attributed to its serine protease activity. Both *in vivo* and *in vitro* experiments provided further evidence, showing that the protective effect of NK was significantly attenuated by heat-inactivated NK or coinubation with PMSF. Additionally, we employed proteomics to analyze brain proteins affected by NK, revealing a predominant impact on proteins associated with inflammation and coagulation, consistent with the general findings of this study. These results provide crucial insights into the intricate mechanisms underpinning NK's protective effects in the context of IS.

Taken together, our study elucidated the protective impact of NK on IS. Using comprehensive *in vivo* and *in vitro* approaches, we robustly demonstrated NK's ability to mitigate microglial inflammation and neurons' OGD/R injury, indicating NK's multifaceted protective effects. Mechanically, NK exerted its protective influence through enzymatic degradation of TLR4. Consequently, these investigations strongly advocate for NK as a promising candidate for therapeutic interventions in IS, presenting a novel avenue in the development of pharmaceutical treatments.

## Materials & Methods

### Chemicals and reagents

Nattokinase (2000 FU/mg) was acquired from Sungen Biotech (Shantou, Guangdong, China). Dulbecco's modified Eagle's medium (DMEM) and fetal bovine serum (FBS) were obtained from Life Technologies/Gibco Laboratories (Grand Island, NY, USA). The antibodies in this study were as follows: p-I $\kappa$ B- $\alpha$  (AF2002), GRP78 (AF0729), CHOP (AF6277), BAX (AF0120), Bcl2 (AF6139), Beclin1 (AF5128), p65 (AF5006), IBA1 (DF6442), Goat anti-rabbit IgG (H + L) HRP (S0001), and  $\beta$ -actin (AF7018), which were purchased from Affinity Biosciences (Cincinnati, OH, USA). LC3 (A11280) and p62 (A19700) were purchased from ABclonal Technology (Wuhan, China). Furthermore, Toll-like receptor 4 (TLR4, GB11519) antibodies were supplied by Servicebio Co., Ltd. (Wuhan, China). PAR (E6F6A) and Caspase3 (D3R6Y) antibodies were purchased from Cell Signaling Technology (Boston, MA, USA). Electronic laboratory notebook was not used for recording experimental procedures and results. Instead, all experimental procedures and data were recorded manually in a traditional laboratory notebook.

### Animals and ethics

Eight-week-old Sprague Dawley (SD) rats (male, weight 180–220 g) were sourced from the Experimental Animal Center of Shenyang Pharmaceutical University (Shenyang, China) and maintained under standard housing conditions in a 12-h light–12-h dark cycle with free access to food and water. Animal experiments were designed according to the guidelines of the animal facility of Shenyang Pharmaceutical University and approved by the Institutional Ethics Committee and were carried out to minimize the number of animals used and the suffering caused by the procedures used in this study.

### Transient Middle cerebral artery occlusion (tMCAO) surgery

A total of 155 eight-week-old Sprague Dawley (SD) rats (male, weight 180–220 g) were purchased from Liaoning Changsheng Biotechnology Co., Ltd. A total of 17 rats that died after ischemia and six rats that failed to induced ischemia were excluded (Exclusion criteria: Died during the surgical operation and the follow-up period before the neurological examination). After 7–10 days of adaptive feeding, rats were randomly divided into 5 groups: a sham operation group, a tMCAO model group, and three groups treated with NK (5000, 10000, and 20000 FU/kg) when their body weight reached 230–260 g. NK was dissolved in normal saline. Rats were administrated orally with indicated doses of NK or normal saline for 7 days before operation of the tMCAO model. The tMCAO model was described by Longa with modification (Longa et al., 1989). Briefly, a 0.34 mm diameter filament (Beijing Cinontech Co. Ltd.) coated with poly (L-lysine) was inserted into the internal carotid artery (ICA) through the right common carotid artery (CCA). The filament was then advanced further into the ICA until it reached the middle cerebral artery (MCA), approximately 18.0  $\pm$  0.5 mm from the bifurcation of the carotid artery, to ensure the occlusion of the MCA. The filament was secured

around the distal CCA. After 2 h of MCAO, blood flow was restored by removing the suture. In the Sham group, the right common carotid artery was exposed using the same method without further intervention.

The anesthesia protocol used for tMCAO survival surgery and euthanasia involved the administration of isoflurane. For survival surgery, animals were initially anesthetized with 3–5% isoflurane in a mixture of oxygen and air *via* a vaporizer until a surgical plane of anesthesia was achieved. Maintenance anesthesia during surgery was maintained with 1–2% isoflurane. Euthanasia was performed under deep anesthesia induced by 5% isoflurane followed by cessation of the anesthesia supply, ensuring humane and painless euthanasia. During surgery, rectal temperature was maintained at 37°C ±0.5°C using a temperature-regulating heating pad. Following 2 h of ischemia and 24 h of reperfusion, the rats were sacrificed, and brain tissues were collected. All behavioral evaluation of the experimental animals were conducted by researchers who did not know the treatment of each animal.

### Behavioral tests

Behavioral tests were employed to assess the neurological function recovery of animals after I/R, including the mNSS, the cylinder test, and the rotarod test. The mNSS consisted of various evaluations, including motor functions, sensory functions, balancing functions, and reflex functions, and abnormal movements. The total score of the mNSS ranged from 0 to 18, with higher scores indicating more severe deficits (Supplementary Table S1), as previously reported (Shen et al., 2006; Wang et al., 2022a). Two independent investigators, who were blinded to the groupings of animals, performed the assessment of neurological function. In case of disagreement, consensus was reached regarding the subitem and the total score.

To evaluate motor function, the forelimb asymmetry test was performed (Hua et al., 2005). The rats were trained for this test twice daily for 3 days before surgery and subjected to the test at 24 h after reperfusion. The test involved placing rats in a transparent glass cylinder (diameter: 20 cm, height: 30 cm, without lid) and closely monitoring their behavior. Once each rat had adapted to the environment and started moving, the number of simultaneous and individual wall contacts made by both forelimbs was observed for 5 min and recorded. Simultaneous wall contact was defined as one limb touching the wall first, followed immediately by the other limb. The utilization of the left forelimb was calculated as follows: (number of wall touches with left limb + 1/2 number of wall touches on both sides)/(number of wall touches with left limb + number of wall touches with right limb + number of wall touches on both sides) × 100%. These steps were repeated three times at intervals of more than 5 min to ensure consistency and accuracy in the evaluation.

Rotarod test was performed to evaluate motor function of rats by using an accelerating rotarod (ITC Life Science Inc. CA, USA). Rats were trained for 3 days with 3 trails per day before doing the tests to obtain stable baselines. The initial speed of the rod was 10 rounds per min, and it gradually speeded up to 30 rounds/min after 100 s. Only rats that stayed on the rods for 80–100 s were included for further experiments. A trial ended if the animal fell off from the

rods or gripped the device and spun around for two consecutive rotations without attempting to walk on rod. Durations of three trails were collected for data analysis. Rats were subjected to rotarod test at 24 h after tMCAO surgery.

### Triphenyltetrazolium chloride staining

Following the assessment of neurological deficits, the rats were humanely euthanized under deep anesthesia and the brain tissues were carefully extracted. After removing the olfactory bulb, cerebellum, and lower brainstem, the brain tissues underwent a brief period of freezing in the refrigerator for 30 min. Subsequently, the brain tissue was sectioned into 5 slices using a precise knife. These brain slices were subjected to staining with a 1% solution of 2,3,5-triphenyltetrazolium chloride solution (TTC, Tetrazolium Red, MB2599-1, Meilunbio, Dalian, China) in a dark constant temperature water bath at 37°C for 20 min. The images of the stained brain slices were captured by a digital camera and analyzed using ImageJ software to determine the infarct volumes. TTC staining showed that normal brain tissues exhibited a rose-red coloration and infarcted brain tissues identified by the white appearance.

### Brain water content measurement

Brain edema was determined with the wet–dry method 24 h after MCAO. Briefly, rats were sacrificed by decapitation under deep anesthesia, and the brain was quickly removed. Tissue samples were dissected and weighed immediately to obtain wet weight. Dry weight was determined after heating the tissue for 48 h at 100°C. Brain water content was then calculated using the following formula: % H<sub>2</sub>O = (1-dry weight/wet weight) × 100%.

### Nissl staining

The slides were baked at 60°C for 30 min and conventional dewaxing was carried out in xylene solution and gradient alcohol solution. The Tar Violet staining solution was placed in a 56°C incubator for 1 h of preheating. The dewaxed sections were put into the preheated Tar Violet staining solution and stained for 10 min. After washing with deionized water, the slides were placed in Nissl differentiation solution for differentiation for 1 min. After staining, the slides were placed in the gradient ascending alcohol solution and xylene solution for dehydration and transparency. A neutral adhesive was used to seal the sheet and the results were observed and the photographs were taken under a microscope (BX60; Olympus, Japan).

### Microglia morphology analysis

The extent of ramified microglial morphology was quantified using an objective and computer-aided skeleton analysis method as previously published in detail (Young and Morrison, 2018). A series of ImageJ plugins (*i.e.*, adjust brightness, unsharp mask, and Despeckle) were temporarily applied to ensure adequate cell process visualization before the conversion to binary and skeletonized images. The skeletonized representations of original photomicrographs were used for data collection of two parameters: the number of endpoints/cell and process length/cell. The Analyze Skeleton

(2D/3D) plugin (developed and maintained by Arganda-Carreras et al., 2010) was used to tag elements of microglial skeletons as processes (orange slab voxels) and endpoints (blue) for data collection. We summarized the number of endpoints and process length from Analyze Skeleton (2D/3D) plugin data output, and all data were divided by cell soma counts, an approximation of the number of cells imaged in each frame.

### ELISA

Briefly, brain homogenate was obtained from infarct sites by tissue homogenizer and centrifuged at 12,000 rpm for 10 min to keep the supernatant. Total protein concentration in brain homogenates was adjusted to 1 mg/mL. Serum samples were isolated by centrifugation (4°C, 15 min, 1500 rpm), collated as supernatant. Enzyme-linked immunosorbent assay (ELISA) was performed using commercially available kits for ELISA. The TNF- $\alpha$  and IL-10 were purchased from Shanghai Ruifan Biotechnology CO.,LTD (Shanghai Chain), thrombin, tPA, FIB, and PAI1 were supplied by Beyotime (Shanghai, China). The inflammatory factors of cells were detected of the culture supernatant.

### Measurements of MDA, SOD, and T-AOC levels

The levels of MDA, SOD, and T-AOC were analyzed using specific assay kits according to the manufacturer's instructions (Nanjing Jiancheng Bioengineering Institute, Nanjing, China).

### Cell culture

The immortalized murine microglial cell line BV2 and neuroblastoma cells SH-SY5Y were purchased from the Cell Bank of the Chinese Academy of Sciences (Shanghai, China). These cell lines were cultured in DMEM supplemented with 10% FBS at 37°C in a humidified atmosphere of 5% CO<sub>2</sub> in an incubator. To establish the LPS model, BV2 cells were treated with 1  $\mu$ g/mL LPS (L2630, Sigma-Aldrich, USA) to activate microglial cells. Different concentrations of NK were applied for 2 h before LPS treatment. For the OGD/R model in SH-SY5Y cells, the cell growth medium was replaced with glucose-free medium. Subsequently, the cells were enclosed within an anaerobic chamber equipped with iron and activated carbon package. This packaging efficiently depleted the chamber of oxygen by interacting with the water inside the activated carbon and the ambient oxygen in the chamber. Once tightly sealed, it was incubated at 37°C for 2 h, followed by reoxygenation and glucose for 24 h. The coculture system consisted of SH-SY5Y cells and BV2 cells in a 3:1 ratio. Cells were pretreated with NK (0.06 FU/mL) for 2 h and then exposed to LPS (0.1  $\mu$ g/mL) for 24 h.

### Transwell assay

Transwell chambers (LABSELECT, China) with 0.4  $\mu$ m pores were used to explore the connection between HT22 with BV2 cells, allowing the transfer of molecules or substances from one cell to another without direct physical contact between the cells. Notably, BV2 and HT22 cells were cultured separately in the upper insert chamber and the lower

six-well plate. After 24 h, the insert membranes of BV2 cells were assembled to the wells where HT22 cells were plated. The cocultures of BV2 cells on the insert membrane and HT22 cells on the bottom were pretreated with NK (0.06 FU/mL) for 2 h before LPS (0.1  $\mu$ g/mL) for 24 h. Then the medium was collected to determine the secretion of inflammatory factors by ELISA, the upper layer BV2 cells were used to test the phenotypic switching by qPCR, and the lower layer HT22 cells were used to detect the cell death by AO/PI staining.

### Primary astrocyte culture and treatment

Primary astrocytes were prepared from cerebral cortices of one-day-old neonatal Sprague Dawley rats. Briefly, cerebral cortices of the pups were isolated in ice-cold Hank's Balanced Salt Solution, and meninges were removed. The tissue was then digested in 0.125% trypsin at 37°C for 15 min before DMEM with 10% FBS was added. After homogenization by pipetting 100 times, the mixture was filtered through a cell strainer and centrifuged at 200 g for 5 min. The cells were resuspended by DMEM containing 10% FBS and penicillin-streptomycin and seeded in cell flask coated with Poly-L-Lysine (P4832, Sigma-Aldrich, USA) overnight. Subsequently, the medium was replaced to remove nonadherent cells. After that, half of the medium was changed every 3 days. When the mixed cell culture reached confluence, astrocytes were isolated by shaking the flasks at 37°C at 300 rpm for 4–6 h. The adherent cells were washed by PBS twice and dissociated by 0.25% trypsin for 2 min at 37°C, centrifuged at 200 g for 5 min, and then seeded in cell culture dishes. Half of the medium was renewed every 3 days. Astrocyte cells were treated with 0.1  $\mu$ g/mL LPS to activate cells. Different concentrations of NK were applied for 2 h before LPS treatment. The content of TNF- $\alpha$  and IL-10 were performed using commercially available kits for ELISA (Ruifan, Shanghai, China).

### Nitrite determination and MTT assay

The production of nitric oxide (NO) was assessed by measuring the accumulation of its stable end product, nitrite (NO<sup>2-</sup>), in the culture medium using Griess reagent. Briefly, equal amounts of culture supernatant and Griess reagent (1% sulfanilamide in 5% phosphoric acid and 0.1%  $\alpha$ -naphthylethylenediamine dihydrochloride in distilled water) were mixed and incubated for 10 min at room temperature. The reaction was measured at 540 nm on a microplate reader (Microplate Reader Benchmark, Bio-Rad, CA, USA). For the MTT assay, MTT stock solution (5 mg/mL) was added to the cells to equal to one-tenth of the original culture volume and incubated for 4 h. Purple MTT formazan was solubilized with DMSO and measured by microplate reader (492 nm).

### Annexin V staining and flow cytometry

SH-SY5Y cells were seeded in a 6-well plate at a density of  $2.5 \times 10^5$  cells/well. After the specified treatments, an Annexin V-FITC/PI Apoptosis Assay Kit (ELabScience, China) was used to measure apoptosis rates according to the manufacturer's instructions followed by flow cytometry

analysis (Beckman Coulter, USA). Each group was taken in triplicate.

#### *Acridine orange/propidium iodide double fluorescence staining*

Cells ( $2 \times 10^5$  cells/well) were cultured in a 6-well plate and were treated with or without NK (0.06 FU/mL). Twenty-four hours after LPS (0.1  $\mu\text{g}/\text{mL}$ ) treatment, the culture medium was drained and 1 mL of PBS solution containing 1  $\mu\text{L}$  of acridine orange (AO) (1 mg/5 mL) and 1  $\mu\text{L}$  of propidium iodide (PI) (1 mg/3 mL) was added to each well and immediately imaged by fluorescent invert microscope.

#### *Immunofluorescence*

Anesthetized rats were successively administered intracardial perfusion using 0.9% sodium chloride solution and 4% paraformaldehyde (PFA). Brains were meticulously fixed in 4% PFA overnight and then dehydrated using a gradient sucrose solution with concentrations of 10%, 20%, and 30%, all kept at a temperature of 4°C. The brains were embedded in an optimal cutting temperature compound (Sakura Finetek, USA), and sliced into sections measuring 18 mm thickness. For the staining, the sections were blocked with 0.3% Triton, 3% goat serum, and 5% bovine serum albumin for 60 min and then incubated with the indicated primary antibodies at 4°C overnight. The primary antibodies were used at a dilution of 1:200 unless otherwise specified. On the following day, the sections were incubated with secondary antibody and DAPI (Sigma-Aldrich, USA). Secondary antibodies were donkey anti-mouse, anti-rabbit, or anti-rat conjugated with Alexa 488. High-resolution images were captured with the Olympus BX51 microscope (Olympus, Japan).

#### *Determination of ROS*

Cells were cultured in 6-well plates with a density of  $1 \times 10^5$  cells/mL for 24 h. Cells were treated with various concentrations of NK before exposure to LPS (0.1  $\mu\text{g}/\text{mL}$ ) or OGD/R for 24 h. To evaluate the ROS production of rats, the brain was carefully and quickly isolated, cut into 18.0  $\mu\text{m}$  sections and placed on chilled microscope slides. The cells or tissues were then stained with DHE (5  $\mu\text{M}$ ) for 30 min at 37°C in the dark. The cells or brain sections were washed twice with PBS and placed under a confocal microscope.

#### *Western blot*

The samples were separated by sodium dodecyl sulfate-polyacrylamide gel electrophoresis (Affinibody Lifescience, Wuhan, China) and transferred onto polyvinylidene difluoride membranes (EMD Millipore, Billerica, MA, U.S.A.). The membranes were then blocked in rapid blocking buffer (SW152, Seven, Beijing, China) for 10 min at room temperature followed by incubating with the corresponding primary antibodies overnight at 4°C. After thorough washing, the membranes were exposed to secondary antibody coupled with horseradish peroxidase against the primary antibodies at room temperature for 2 h. The immune reaction was developed using the enhanced chemiluminescence reaction (Affinibody Lifescience, Wuhan, China), and the protein

bands were imaged by a ChemiDoc XRS system (Bio-Rad, Hercules, CA, U.S.A.). ImageJ software was utilized for quantification and analysis of protein-level changes.

#### *Quantitative Real-Time PCR*

Total RNA was extracted using TRIzol (Invitrogen) according to the manufacturer's instructions. Rat tissue RNA samples were collected from brain tissues and medium RNA samples were extracted and isolated from BV2 cells. Total RNA was reverse transcribed into cDNAs using a Superscript cDNA Premix Kit II with oligo (dT) primers (Vazyme, Nanjing, China). The real-time PCR reaction was performed on a real-time PCR system (Applied Biosystems, Foster City, CA, USA) with SYBR Green using Prime Taq Premix (TransGen Biotech, China). Actin was used as an internal control for mRNA quantification, threshold cycle (CT) was determined, and relative levels of mRNA was calculated based on the CT values. Data were analyzed using the  $2^{-\Delta\Delta\text{CT}}$  method. The primers of rats used in this study included:

CD206 (forward 5'-TCAGCTATTGGACGCGAGGCA-3', reverse 5'-TCCGGGTTGCAAGTTGCCG-3'),

ARG1 (forward 5'-CAGGGTAATGAGTGGGTTG-3', reverse 5'-CACGGCACCTCCTAAATTG-3'),

CD86 (forward 5'-GACCGTTGTGTGTGTTCTG-3', reverse 5'-GATGAGCAGCATCACAAGG-3'),

iNOS (forward 5'-CAGCTGGGCTGTACAAACCT-3', reverse 5'-CATTGGAAGTGAAGCGTTTC-3'),

and actin (forward 5'-AGCGAGACCCCACTAACAT-3', reverse 5'-GGTTCACACCCATCACAAA-3').

The following primers of cells were used in this study:

CD206 (forward 5'-CCTATGAAAATTGGGCTTACGG-3', reverse 5'-CTGACAAATCCAGTTGTTGAGG-3'),

ARG1 (forward 5'-CATATCTGCCAAAGACATCGTG-3', reverse 5'-GACATCAAAGCTCAGGTGAATC-3'),

CD86 (forward 5'-ACGGAGTCAATGAAGATTTCCT-3', reverse 5'-GATTCGGCTTCTTGTGACATAC-3')

iNOS (forward 5'-CATATCTGCCAAAGACATCGTG-3', reverse 5'-CCAAGCCCCTACCATTTATCT-3'),

TLR4 (forward 5'-GCCATCATTATGAGTGCCAATT-3', reverse 5'-AGGGATAAGAACGCTGAGAATT-3'), and

actin (forward 5'-AGTTCAACGGCACAGTCAAGGC-3', reverse 5'-CGACATACTCAGCACCAGCATCAC-3').

#### *Data-Dependent acquisition proteomics*

Mass spectrometry data were acquired using Data-Dependent Acquisition (DDA) mode scanning, the chromatographic condition of which was consistent with the DDA method. Proteomic analysis was performed using the Q-Exactive HF-X mass spectrometer (Thermo Fisher Scientific, USA) coupled to a Nano-Electrospray Flex Ion Source (Thermo Fisher Scientific, USA). The RAW data files were processed and quantified by Proteome Discoverer software v2.4.1.15 (Thermo Fisher Scientific, Massachusetts, USA), and searched against the RefSeq Human protein database (24078 sequences, release 2017\_03) using the SEQUEST algorithm. Proteins with a fold change greater than 1.5 and a *p* value less than 0.05 were statistically significant. Student *t*-test was used to identify proteins with significantly different expression. Fisher's exact test was used to find enriched

Gene Ontology (GO) (Ashburner et al., 2000) and KEGG (Kanehisa et al., 2004) by differentially expressed proteins.

### Statistical analysis

Data are presented as mean  $\pm$  standard deviation (SD). All expression were checked for normality and lognormality tests, and if data do not meet the criteria for a normal distribution, then a nonparametric test was used. If the data contained three or more groups, one-way analysis of variance followed by multiple comparison tests were used. A *p* value less than 0.05 was considered statistically significant. Data were analyzed using GraphPad Prism 8.0.

### Authors' Contributions

X.Y., S.W., and W.X. conceived and designed the experiments. X.Y., S.W., W.X., and Y.Z. performed the experiments and analyzed the data. X.Y., S.W., L.L., and Z.L. contributed reagents/materials/analysis tools. X.Y. and S.W. wrote the draft, checked, and revised. All authors approved to submit this version of the publication.

### Data Availability Statement

The mass spectrometry proteomics data have been deposited to the ProteomeXchange Consortium (<https://proteomecentral.proteomexchange.org>) via the iProX partner repository (Chen et al., 2022, Ma et al., 2019) with the dataset identifier PXD052988.

### Author Disclosure Statement

The authors declare no potential conflicts of interest with respect to the research, authorship, and/or publication of this article.

### Funding Information

This research did not receive any specific grant from funding agencies in the public, commercial, or not-for-profit sectors.

### Supplementary Material

Supplementary Figure S1  
Supplementary Figure S2  
Supplementary Figure S3  
Supplementary Table S1

### References

- Ajoolabady A, Wang S, Kroemer G, et al. Targeting autophagy in ischemic stroke: From molecular mechanisms to clinical therapeutics. *Pharmacol Ther* 2021;225:107848; doi: 10.1016/j.pharmthera.2021.107848
- Arganda-Carreras I, Fernández-González R, Muñoz-Barrutia A, et al. 3D reconstruction of histological sections: Application to mammary gland tissue. *Microsc Res Tech* 2010;73(11):1019–1029; doi: 10.1002/jemt.20829
- Ashburner M, Ball CA, Blake JA, et al. Gene ontology: Tool for the unification of biology. The gene ontology consortium. *Nat Genet* 2000;25(1):25–29; doi: 10.1038/75556
- Aslanidis A, Karlstetter M, Scholz R, et al. Activated microglia/macrophage whey acidic protein (AMWAP) inhibits NF $\kappa$ B signaling and induces a neuroprotective phenotype in microglia. *J Neuroinflammation* 2015;12:77; doi: 10.1186/s12974-015-0296-6
- Barton GM, Kagan JC. A cell biological view of toll-like receptor function: Regulation through compartmentalization. *Nat Rev Immunol* 2009;9(8):535–542; doi: 10.1038/nri2587
- Bredesen DE, Rao RV, Mehlen P. Cell death in the nervous system. *Nature* 2006;443(7113):796–802; doi: 10.1038/nature05293
- Calabrese V, Cornelius C, Dinkova-Kostova AT, et al. Cellular stress responses, the hormesis paradigm, and vitagenes: Novel targets for therapeutic intervention in neurodegenerative disorders. *Antioxid Redox Signal* 2010;13(11):1763–1811; doi: 10.1089/ars.2009.3074
- Calabrese V, Giordano J, Signorile A, et al. Major pathogenic mechanisms in vascular dementia: Roles of cellular stress response and hormesis in neuroprotection. *J Neurosci Res* 2016;94(12):1588–1603; doi: 10.1002/jnr.23925
- Calabrese V, Mancuso C, Calvani M, et al. Nitric oxide in the central nervous system: Neuroprotection versus neurotoxicity. *Nat Rev Neurosci* 2007;8(10):766–775; doi: 10.1038/nrn2214
- Caso JR, Pradillo JM, Hurtado O, et al. Toll-like receptor 4 is involved in brain damage and inflammation after experimental stroke. *Circulation* 2007;115(12):1599–1608; doi: 10.1161/circulationaha.106.603431
- Chanchal S, Mishra A, Singh MK, et al. Understanding inflammatory responses in the manifestation of prothrombotic phenotypes. *Front Cell Dev Biol* 2020;8:73; doi: 10.3389/fcell.2020.00073
- Chen T, Ma J, Liu Y, et al. iProX in 2021: Connecting proteomics data sharing with big data. *Nucleic Acids Res* 2022; 50(D1):D1522–D1527; doi: 10.1093/nar/gkab1081
- Concetta Scuto M, Mancuso C, Tomasello B, et al. Curcumin, hormesis and the nervous system. *Nutrients* 2019;11(10); doi: 10.3390/nu11102417
- D'Amico R, Trovato Salinaro A, Fusco R, et al. *Hericium erinaceus* and *coriolus versicolor* modulate molecular and biochemical changes after traumatic brain injury. *Antioxidants (Basel)* 2021;10(6); doi: 10.3390/antiox10060898
- de Zoete MR, Bouwman LI, Keestra AM, et al. Cleavage and activation of a Toll-like receptor by microbial proteases. *Proc Natl Acad Sci U S A* 2011;108(12):4968–4973; doi: 10.1073/pnas.1018135108
- Ewald SE, Lee BL, Lau L, et al. The ectodomain of toll-like receptor 9 is cleaved to generate a functional receptor. *Nature* 2008;456(7222):658–662; doi: 10.1038/nature07405
- Goldmann T, Wieghofer P, Müller PF, et al. A new type of microglia gene targeting shows TAK1 to be pivotal in CNS autoimmune inflammation. *Nat Neurosci* 2013;16(11):1618–1626; doi: 10.1038/nn.3531
- Guo YL, Duan WJ, Lu DH, et al. Autophagy-dependent removal of  $\alpha$ -synuclein: A novel mechanism of GM1 ganglioside neuroprotection against Parkinson's disease. *Acta Pharmacol Sin* 2021;42(4):518–528; doi: 10.1038/s41401-020-0454-y
- Herpich F, Rincon F. Management of acute ischemic stroke. *Crit Care Med* 2020;48(11):1654–1663; doi: 10.1097/ccm.0000000000004597
- Hua Y, Wu J, Pecina S, et al. Ischemic preconditioning procedure induces behavioral deficits in the absence of brain injury? *Neurol Res* 2005;27(3):261–267; doi: 10.1179/016164105x25270

- Iadecola C, Anrather J. Stroke research at a crossroad: Asking the brain for directions. *Nat Neurosci* 2011;14(11):1363–1368; doi: 10.1038/nn.2953
- Kanazawa M, Ninomiya I, Hatakeyama M, et al. Microglia and monocytes/macrophages polarization reveal novel therapeutic mechanism against stroke. *Int J Mol Sci* 2017;18(10); doi: 10.3390/ijms18102135
- Kanehisa M, Goto S, Kawashima S, et al. The KEGG resource for deciphering the genome. *Nucleic Acids Res* 2004; 32(Database issue):D277–D280; doi: 10.1093/nar/gkh063
- Kim J, Gum S, Paik J, et al. Effects of nattokinase on blood pressure: A randomized, controlled trial. *Hypertens Res* 2008;31(8):1583–1588; doi: 10.1291/hypres.31.1583
- Koehler RC, Dawson VL, Dawson TM. Targeting parthanatos in ischemic stroke. *Front Neurol* 2021;12:662034; doi: 10.3389/fneur.2021.662034
- Levi M, van der Poll T. Inflammation and coagulation. *Crit Care Med* 2010;38(Suppl 2):S26–S34; doi: 10.1097/CCM.0b013e3181c98d21
- Levi M, van der Poll T, Büller HR. Bidirectional relation between inflammation and coagulation. *Circulation* 2004; 109(22):2698–2704; doi: 10.1161/01.CIR.0000131660.51520.9A
- Li Q, Barres BA. Microglia and macrophages in brain homeostasis and disease. *Nat Rev Immunol* 2018;18(4):225–242; doi: 10.1038/nri.2017.125
- Li Y, Zhang Y, Fu H, et al. Hes1 knockdown exacerbates ischemic stroke following tMCAO by increasing ER stress-dependent apoptosis via the PERK/eIF2 $\alpha$ /ATF4/CHOP signaling pathway. *Neurosci Bull* 2020;36(2):134–142; doi: 10.1007/s12264-019-00411-7
- Lin YW, Chen TY, Hung CY, et al. Melatonin protects brain against ischemia/reperfusion injury by attenuating endoplasmic reticulum stress. *Int J Mol Med* 2018;42(1):182–192; doi: 10.3892/ijmm.2018.3607
- Lin D, Wang L, Yan S, et al. The role of oxidative stress in common risk factors and mechanisms of cardio-cerebrovascular ischemia and depression. *Oxid Med Cell Longev* 2019;2019:2491927; doi: 10.1155/2019/2491927
- Longa EZ, Weinstein PR, Carlson S, et al. Reversible middle cerebral artery occlusion without craniectomy in rats. *Stroke* 1989;20(1):84–91; doi: 10.1161/01.str.20.1.84
- Ma J, Chen T, Wu S, et al. iProX: An integrated proteome resource. *Nucleic Acids Res* 2019;47(D1):D1211–D1217; doi: 10.1093/nar/gky869
- Mancuso C, Capone C, Ranieri SC, et al. Bilirubin as an endogenous modulator of neurotrophin redox signaling. *J Neurosci Res* 2008;86(10):2235–2249; doi: 10.1002/jnr.21665
- Masselli E, Pozzi G, Vaccarezza M, et al. ROS in platelet biology: Functional aspects and methodological insights. *Int J Mol Sci* 2020;21(14); doi: 10.3390/ijms21144866
- McDonald B, Davis RP, Kim SJ, et al. Platelets and neutrophil extracellular traps collaborate to promote intravascular coagulation during sepsis in mice. *Blood* 2017;129(10):1357–1367; doi: 10.1182/blood-2016-09-741298
- Nam M, Shin H, Han J, et al. Essential roles of mitochondrial depolarization in neuron loss through microglial activation and attraction toward neurons. *Brain Res* 2013;1505:75–85; doi: 10.1016/j.brainres.2013.02.005
- Onose G, Anghelescu A, Blendea D, et al. Cellular and molecular targets for non-invasive, non-pharmacological therapeutic/rehabilitative interventions in acute ischemic stroke. *Int J Mol Sci* 2022;23(2); doi: 10.3390/ijms23020907
- Opal SM, Esmon CT. Bench-to-bedside review: Functional relationships between coagulation and the innate immune response and their respective roles in the pathogenesis of sepsis. *Crit Care* 2003;7(1):23–38; doi: 10.1186/cc1854
- Poh L, Kang SW, Baik SH, et al. Evidence that NLRC4 inflammasome mediates apoptotic and pyroptotic microglial death following ischemic stroke. *Brain Behav Immun* 2019;75:34–47; doi: 10.1016/j.bbi.2018.09.001
- Rajan WD, Wojtas B, Gielniewski B, et al. Dissecting functional phenotypes of microglia and macrophages in the rat brain after transient cerebral ischemia. *Glia* 2019;67(2):232–245; doi: 10.1002/glia.23536
- Ransohoff RM. A polarizing question: Do M1 and M2 microglia exist? *Nat Neurosci* 2016;19(8):987–991; doi: 10.1038/nn.4338
- Rao Y, Du S, Yang B, et al. NeuroD1 induces microglial apoptosis and cannot induce microglia-to-neuron cross-lineage reprogramming. *Neuron* 2021;109(24):4094–4108.e4095; doi: 10.1016/j.neuron.2021.11.008
- Richards LG, Cramer SC. Therapies targeting stroke recovery. *Stroke* 2023;54(1):265–269; doi: 10.1161/strokeaha.122.041729
- Sarvari S, Moakedi F, Hone E, et al. Mechanisms in blood-brain barrier opening and metabolism-challenged cerebrovascular ischemia with emphasis on ischemic stroke. *Metab Brain Dis* 2020;35(6):851–868; doi: 10.1007/s11011-020-00573-8
- Shen LH, Li Y, Chen J, et al. Intracarotid transplantation of bone marrow stromal cells increases axon-myelin remodeling after stroke. *Neuroscience* 2006;137(2):393–399; doi: 10.1016/j.neuroscience.2005.08.092
- Stoll G, Nieswandt B. Thrombo-inflammation in acute ischemic stroke—implications for treatment. *Nat Rev Neurol* 2019;15(8):473–481; doi: 10.1038/s41582-019-0221-1
- Sumii T, Lo EJS. Involvement of matrix metalloproteinase in thrombolysis-associated hemorrhagic transformation after embolic focal ischemia in rats. *Stroke* 2002;33(3):831–836; doi: 10.1161/hs0302.104542
- Tang J, Xiang Z, Bernards MT, et al. Peritoneal adhesions: Occurrence, prevention and experimental models. *Acta Biomater* 2020;116:84–104; doi: 10.1016/j.actbio.2020.08.036
- Tsantarliotou MP, Lavrentiadou SN, Psalla DA, et al. Suppression of plasminogen activator inhibitor-1 (PAI-1) activity by crocin ameliorates lipopolysaccharide-induced thrombosis in rats. *Food Chem Toxicol* 2019;125:190–197; doi: 10.1016/j.fct.2019.01.001
- Tuo QZ, Zhang ST, Lei P. Mechanisms of neuronal cell death in ischemic stroke and their therapeutic implications. *Med Res Rev* 2022;42(1):259–305; doi: 10.1002/med.21817
- Wang L, Duan Z, Liang M, et al. A pivotal role of selective autophagy in mitochondrial quality control: Implications for zinc oxide nanoparticles induced neurotoxicity. *Chem Biol Interact* 2022b;363:110003; doi: 10.1016/j.cbi.2022.110003
- Wang X, Fang Y, Huang Q, et al. An updated review of autophagy in ischemic stroke: From mechanisms to therapies. *Exp Neurol* 2021;340:113684; doi: 10.1016/j.expneurol.2021.113684
- Wang W, Li M, Chen Q, et al. Hemorrhagic transformation after tissue plasminogen activator reperfusion therapy for ischemic stroke: Mechanisms, models, and biomarkers. *Mol Neurobiol* 2015;52(3):1572–1579; doi: 10.1007/s12035-014-8952-x
- Wang P, Liang J, Li Y, et al. Down-regulation of miRNA-30a alleviates cerebral ischemic injury through enhancing beclin 1-mediated autophagy. *Neurochem Res* 2014;39(7):1279–1291; doi: 10.1007/s11064-014-1310-6
- Wang HJ, Ran H-F, Yin Y, et al. Catalpol improves impaired neurovascular unit in ischemic stroke rats via enhancing

- VEGF-PI3K/AKT and VEGF-MEK1/2/ERK1/2 signaling. *Acta Pharmacol Sin* 2022a;43(7):1670–1685; doi: 10.1038/s41401-021-00803-4
- Wang D, Yang Y, Wang Y, et al. Embelin ameliorated sepsis-induced disseminated intravascular coagulation intensities by simultaneously suppressing inflammation and thrombosis. *Biomed Pharmacother* 2020;130:110528; doi: 10.1016/j.biopha.2020.110528
- Wu H, Wang H, Li W, et al. Nattokinase-heparin exhibits beneficial efficacy and safety-an optimal strategy for CKD patients on hemodialysis. *Glycoconj J* 2019;36(2):93–101; doi: 10.1007/s10719-019-09860-8
- Wu H, Wang H, Xu F, et al. Acute toxicity and genotoxicity evaluations of Nattokinase, a promising agent for cardiovascular diseases prevention. *Regul Toxicol Pharmacol* 2019; 103:205–209; doi: 10.1016/j.yrtph.2019.02.006
- Wu H, Wang Y, Zhang Y, et al. Breaking the vicious loop between inflammation, oxidative stress and coagulation, a novel anti-thrombus insight of nattokinase by inhibiting LPS-induced inflammation and oxidative stress. *Redox Biol* 2020; 32:101500; doi: 10.1016/j.redox.2020.101500
- Wu H, Zhang Q, Xu P, et al. Nattokinase promotes post-stroke neurogenesis and cognition recovery via increasing circulating Irisin. *J Agric Food Chem* 2023;71(30):11418–11428; doi: 10.1021/acs.jafc.2c08718
- Wu H, Zheng J, Xu S, et al. Mer regulates microglial/macrophage M1/M2 polarization and alleviates neuroinflammation following traumatic brain injury. *J Neuroinflammation* 2021; 18(1):2; doi: 10.1186/s12974-020-02041-7
- Xu SY, Pan SY. The failure of animal models of neuroprotection in acute ischemic stroke to translate to clinical efficacy. *Med Sci Monit Basic Res* 2013;19:37–45; doi: 10.12659/msmbr.883750
- Yamaguchi Y, Miura M. Programmed cell death in neurodevelopment. *Dev Cell* 2015;32(4):478–490; doi: 10.1016/j.devcel.2015.01.019
- Young K, Morrison H. Quantifying microglia morphology from photomicrographs of immunohistochemistry prepared tissue using imageJ. *J Vis Exp* 2018;(136):57648; doi: 10.3791/57648
- Zabel MK, Kirsch WM. From development to dysfunction: Microglia and the complement cascade in CNS homeostasis. *Ageing Res Rev* 2013;12(3):749–756; doi: 10.1016/j.arr.2013.02.001

Address correspondence to:  
 Prof. Feng-jiao Zhang  
 Wuya College of Innovation  
 Shenyang Pharmaceutical University  
 103 Wenhua Road  
 Shenyang 110016  
 China

E-mail: zhangfengjiao82@hotmail.com

Date of first submission to ARS Central, December 9, 2023; date of final revised submission, June 12, 2024; date of acceptance, June 22, 2024.

#### Abbreviations Used

CCA	= common carotid artery
DDA	= data-dependent acquisition
DEGs	= differentially expressed genes
DHE	= dihydroergotamine
DMEM	= Dulbecco's modified Eagle's medium
FBS	= fetal bovine serum
iNOS	= inducible nitric oxide synthase
ICA	= internal carotid artery
IS	= ischemic stroke
IL	= interleukin
KEGG	= Kyoto Encyclopedia of Genes and Genomes
LPS	= lipopolysaccharides
mNSS	= modified neurological severity score
MCA	= middle cerebral artery
NF- $\kappa$ B	= nuclear factor- $\kappa$ B
NO	= nitric oxide
NK	= Nattokinase
OGD/R	= oxygen glucose deprivation/reperfusion
PAI-1	= plasminogen activator inhibitor-1
PFA	= paraformaldehyde
PVDF	= polyvinylidene difluoride
ROS	= reactive oxygen species
tMCAO	= transient middle cerebral artery occlusion
tPA	= tissue plasminogen activator
TLR4	= toll-like receptor 4
TNF- $\alpha$	= tumor necrosis factor- $\alpha$
UPR	= unfolded protein response